# Light-independent regulation of algal photoprotection by $CO_2$ availability


**Authors**

M. Águila Ruiz-Sola[1,†,‡], Serena Flori[1,†], Yizhong Yuan[1,†], Gaelle Villain[1], Emanuel Sanz-Luque[2,3], Petra Redekop[2], Ryutaro Tokutsu[4], Anika Kueken[5,6], Angeliki Tsichla[1], Georgios Kepesidis[1], Guillaume Allorent[1], Marius Arend[5,6], Fabrizio Iacono[1], Giovanni Finazzi[1], Michael Hippler[7], Zoran Nikoloski[5,6], Jun Minagawa[4], Arthur R. Grossman[2], Dimitris Petroutsos[1, *]

**Affiliations**

[1]Univ. Grenoble Alpes, CNRS, CEA, INRAE, IRIG-LPCV, 38000 Grenoble, France

[2]The Carnegie Institution for Science, Department of Plant Biology, Stanford, CA 94305, USA

[3]University of Cordoba, Department of Biochemistry and Molecular Biology, Cordoba, Spain

[4]Division of Environmental photobiology, National Institute for Basic Biology (NIBB), Nishigonaka 38, Myodaiji, Okazaki 444-8585, Japan

[5]Bioinformatics Group, Institute of Biochemistry and Biology, University of Potsdam, Potsdam, Germany.

[6]Max-Planck-Institute of Molecular Plant Physiology, Potsdam, Golm, Germany

[7]Institute of Plant Biology and Biotechnology, Westfälische Wilhelms Universität, 48143 Münster, Germany

[†] these authors contributed equally to this work

[‡] Current address: Instituto de Bioquímica Vegetal y Fotosíntesis, Universidad de Sevilla-CSIC, 41092, Sevilla, Spain and Departamento de Bioquímica Vegetal y Biología Molecular, Facultad de Biología, Universidad de Sevilla, 41012 Sevilla, Spain.

[*]Corresponding Author. Email: dimitrios.petroutsos@cnrs.fr

**Abstract**

Photosynthetic algae have evolved mechanisms to cope with suboptimal light and $CO_2$ conditions. When light energy exceeds $CO_2$ fixation capacity, *Chlamydomonas reinhardtii* activates photoprotection, mediated by LHCSR1/3 and PSBS, and the $CO_2$ Concentrating Mechanism (CCM). How light and $CO_2$ signals converge to regulate these processes remains unclear. Here, we show that excess light activates photoprotection- and CCM-related genes by altering intracellular $CO_2$ concentrations and that depletion of $CO_2$ drives these responses, even in total darkness. High $CO_2$ levels, derived from respiration or impaired photosynthetic fixation, repress *LHCSR3*/CCM genes while stabilizing the LHCSR1 protein. Finally, we show that the CCM regulator CIA5 also regulates photoprotection, controlling *LHCSR3* and *PSBS* transcript accumulation while inhibiting LHCSR1 protein accumulation. This work has allowed us to dissect the effect of $CO_2$ and light on CCM and photoprotection, demonstrating that light often indirectly affects these processes by impacting intracellular $CO_2$ levels.

## Introduction

A major challenge for photosynthetic organisms is to efficiently acclimate to highly dynamic light and nutrient conditions that occur in natural environments. While light provides the energy that fuels photosynthetic $CO_2$ fixation, excess light can cause oxidative damage and ultimately result in cell death. Therefore, light absorption must be precisely managed via photoprotective mechanisms that help integrate the use of light energy with $CO_2$ availability and the potential of the organism to grow and store fixed carbon. A dominant photoprotective mechanism, called qE (energy dependent quenching), results in the harmless dissipation of excess absorbed light energy as heat[1,2]. Triggering qE requires the synthesis of specific proteins and pigments that are controlled both transcriptionally and post-transcriptionally.

In the green microalga *Chlamydomonas reinhardtii* (hereafter *Chlamydomonas*), qE depends on the nucleus-encoded, chloroplast-localized Light Harvesting Complex-Stress Related (LHCSR) proteins LHCSR1, LHCSR3 and Photosystem II Subunit S, PSBS, which are present in many algae and lower plants[3] and belong to the Light Harvesting Complex protein superfamily[4]. The *LHCSR3.1* and *LHCSR3.2* genes in *Chlamydomonas* encode identical LHCSR3 proteins[5], while *PSBS1* and *PSBS2* encode proteins that differ by only one amino acid of the chloroplast transit peptide[6]. While LHCSR1 and LHCSR3 are present in algae but not in vascular plants, PSBS is present in both[4]. PSBS in *Chlamydomonas* is transiently expressed in cells exposed to high light (HL)[6,7] and accumulates in cells exposed to UV-B irradiation[8]. LHCSR3 is the main qE effector protein in HL[5], although LHCSR1 can significantly contribute to qE under certain conditions[9]. In *Chlamydomonas*, expression of *LHCSR3* has been reported to increase upon absorption of blue-light by the photoreceptor phototropin (PHOT1)[10] and involves calcium ion signaling[11], active photosynthetic electron transport (PET)[10,11] and the transcriptional factor CONSTANS, which is also required for activation of the *LHCSR1* and *PSBS* genes[12,13].

Similar to the dynamic light cue, the concentration of inorganic carbon ($HCO_3^-$, $CO_2$ and $CO_3^{2-}$, together designated Ci) in aquatic environments varies spatially and temporally; aquatic $CO_2$ levels can also fluctuate from extremely high (hyper-saturated) to extremely low[14]. Because low $CO_2$ levels limit photoautotrophic growth, microalgae have evolved a $CO_2$ Concentrating Mechanism (CCM) that elevates the level of $CO_2$ at the site of fixation by Ribulose-1,5-bisphosphate carboxylase/oxygenase (RuBisCO). Major components of the CCM are carbonic anhydrases (CAH), which facilitate interconversions among the different Ci species, and Ci transporters. The genes encoding many Ci transporters and CAHs are under the control of the zinc-finger type

79 potential transcription regulator CIA5 (also CCM1)[15,16], which is localized in the nucleus[17] and
80 controls expression of low-$CO_2$ responsive genes.

81 In addition to the use of $CO_2$ to support phototrophic growth in the light, *Chlamydomonas* can also
82 use the two-carbon molecule acetate either in the dark to support heterotrophic growth, or in the
83 light, to support photoheterotrophic or mixotrophic growth[18]. Acetate is incorporated into acetyl-
84 CoA either in a one-step reaction catalyzed by acetyl-CoA synthetase (ACS), or in two steps that
85 use acetate kinase (ACK) and phosphate acetyltransferase (PAT), which sequentially catalyze the
86 formation of acetyl-phosphate and acetyl-CoA[19]. Acetyl-CoA can then enter the glyoxylate cycle,
87 a shunt of the tricarboxylic acid (TCA) cycle[20], recently characterized in *Chlamydomonas* [21], where
88 it can be converted to metabolites that are used for anabolic metabolism. Alternatively, acetyl-CoA
89 enters the TCA cycle to feed the respiratory chain with reducing equivalents. Both, the glyoxylate
90 cycle and respiration are essential for growth in the dark since *Chlamydomonas* mutants affected in
91 either of these processes are unable to grow heterotrophically[21,22].

92 Despite the evident connection between light and $CO_2$ levels, the physiological responses to
93 different light and $CO_2$ availabilities have been traditionally studied separately. However, several
94 lines of evidence indicate that both acetate and Ci abundance impact not only qE but also the
95 establishment of the CCM in *Chlamydomonas*[23-26], while *LHCSR3* transcripts accumulation have
96 been reported to be CIA5-dependent[26-28]. Yet, the mechanism(s) associated with carbon-dependent
97 regulation of qE and CCM induction and the intimate link between the two processes have still not
98 been clearly defined.

99 Here, using genetic and mathematical modelling approaches, we demonstrate that inhibition of
100 LHCSR3 accumulation and CCM activity by acetate is at the level of transcription and a
101 consequence of metabolically produced $CO_2$. We also show that exposure of *Chlamydomonas* to
102 HL triggers not only HL-responses, but also low-$CO_2$ responses, and we report the discovery of a
103 novel $CO_2$- and CIA5-dependent mechanism that activates *LHCSR3* gene expression even in
104 complete darkness. Finally, we propose that PET is critical for activation of *LHCSR3* transcription
105 because it sustains $CO_2$ fixation, consuming intracellular $CO_2$ and thereby relieving its inhibitory
106 effect. This work emphasizes the importance of $CO_2$ in regulating photoprotection and the CCM,
107 and demonstrates that light often indirectly affects these processes by altering intracellular $CO_2$
108 levels.
109
110
111

## Results

### $CO_2$ generated from acetate metabolism inhibits *LHCSR3*

To gain insights into the effect of carbon metabolism on photoprotection, we explored the impact of acetate and high $CO_2$ on *LHCSR3* mRNA and protein levels in wild type (WT) cells and in two mutants impaired in acetate metabolism; the *icl* mutant, which lacks isocitrate lyase, a key enzyme of the glyoxylate cycle[21], and the *dum11* mutant, which is defective in the ubiquinol cytochrome c oxidoreductase (respiratory complex III)[29]. The presence of acetate in the medium of WT cells inhibited accumulation of the *LHCSR3* transcript (**Fig. 1a**, note the logarithmic scale) in both low light (LL) and high light (HL) conditions. No protein was detected in WT under any condition in LL, but inhibition by acetate was apparent in HL (**Fig. 1b**), as previously reported[25]. However, in the *icl* mutant, acetate had no inhibitory effect on accumulation of LHCSR3 mRNA (**Fig. 1a**) or protein (**Fig. 1b**) in either HL or LL, while the *icl::ICL*-complemented line, designated *icl-C*, exhibited similar behavior to that of WT cells (**Fig. 1a** and **b**). Additionally, acetate did not alter LHCSR3 transcript or protein accumulation in HL treated *dum11* mutant cells (**Fig. 1c** and **d)**, while under LL, acetate inhibited *LHCSR3* transcript in the *dum11* mutant but to a much smaller extent than in WT (**Fig. 1c)**. Together, these results suggest that the acetate administered to the cells must be metabolized for it to have a suppressive effect on accumulation of LHCSR3 transcript and protein in HL. We also sparged WT, *icl, icl-C* and *dum11* cells with 5% $CO_2$ both in LL and HL. $CO_2$ strongly repressed accumulation of LHCSR3 mRNA and protein in all genotypes, including the metabolic mutants *icl* and *dum11* for which expression of *LHCSR3* was unaffected by acetate (**Fig. 1a-d**).

We evaluated the impact of carbon availability on the photosynthetic properties of cells. The presence of acetate in the medium of WT cells enhanced photosynthetic electron transport (rETR) and strongly suppressed qE (**Supplementary Fig. 1**). In the *icl* mutant, acetate enhanced the extent of rETR only by ~10% compared with 60% for WT cells. Additionally, acetate caused less pronounced suppression of qE in the *icl* mutant (by 40%) compared to the level of suppression in WT cells (by 95%); *icl-C*, behaved similarly to WT cells. As expected, $CO_2$ enhanced rETR and suppressed qE in WT, *icl* and *icl-C* (S**upplementary Fig. 1**).

The similarity between the impact of acetate and 5% $CO_2$ on *LHCSR3* expression in WT and *icl-C* cells (**Fig. 1a**) as well as on their photosynthetic properties (S**upplementary Fig. 1**) raised the possibility that both treatments elicited a common mechanism of *LHCSR3* control, possibly reflecting a change in the $CO_2$ concentration within the cell or growth medium. This possibility is

145 plausible based on the finding that acetate metabolism leads to the generation of $CO_2$[30]. To
146 investigate whether the generation of $CO_2$ via acetate metabolism can explain repression of
147 LHCSR3 transcript and protein levels, we monitored the levels of transcripts from the *RHP1* gene
148 in the mutant and WT cells; *RHP1* (aka *RH1*) encodes a $CO_2$ channel shown to be $CO_2$ responsive
149 and to accumulate in cells grown in a high $CO_2$ atmosphere[31]. Acetate or 5% $CO_2$ were introduced
150 to WT and *icl* mutant cells acclimated in LL and air and the levels of the *LHCSR3* and *RHP1*
151 transcripts were assayed over a period of 8 h in LL (**Fig. 2a** and **b**). The *LHCSR3* transcript
152 accumulation patterns observed agreed with the findings presented in **Fig. 1a** (LL panel). In WT
153 cells, acetate and $CO_2$ caused a reduction in *LHCSR3* mRNA accumulation over the LL period
154 relative to the control (no acetate, air). Additionally, in the *icl* mutant, acetate did not affect
155 accumulation of this transcript while $CO_2$ efficiently repressed the *LHCSR3* transcript level (**Fig.**
156 **2a**). Under these experimental conditions, acetate levels in the medium decreased in WT cultures
157 but remained unchanged in cultures of the *icl* mutant (**Fig. 2c**). Lastly, *RHP1*expression increased
158 in WT and *icl* mutant cells when the culture was sparged with $CO_2$, but only in the WT cells when
159 the cultures were not sparged with $CO_2$ and only supplemented with acetate, suggesting that acetate
160 metabolism resulted in higher intracellular $CO_2$ levels (**Fig. 2b**).

161 In another experiment, LL acclimated cells were shifted to HL (t=0) and *LHCSR3* and *RHP1*
162 transcript levels were assayed over a period of 9 h; acetate or high $CO_2$ were introduced 1 h after
163 the shift to HL (**Fig. 2d** and **e**, note the 1 h time point highlighted in green on the x-axis). In
164 agreement with **Fig. 1** (HL panel), *LHCSR3* transcript accumulation increased by two orders of
165 magnitude after 1 h exposure to HL in both WT and the *icl* mutant (**Fig. 2d**), while *RHP1* transcripts
166 rapidly decreased **(Fig. 2e)**, which likely resulted from a reduction in the concentration of
167 intracellular $CO_2$ as a consequence of enhanced photosynthetic $CO_2$ fixation in the HL. Introduction
168 of acetate or $CO_2$ to the cultures caused a rapid reduction in the level of *LHCSR3* expression in WT
169 (**Fig. 2d**), with the decline much more pronounced with $CO_2$ supplementation. Supplementation
170 with $CO_2$ or acetate also caused an increase of *RHP1* transcript relative to the control. In contrast,
171 in the *icl* mutant, the decline in the level of the *LHCSR3* transcript and the increase in the level of
172 the *RHP1* transcript was the same in cells with and without acetate supplementation, while the
173 effect of $CO_2$ was similar to that of WT cells (**Fig. 2d** and **e**). Furthermore, WT cells consumed
174 about half of the acetate in the medium over the course of the experiment while none of the acetate
175 was consumed by the *icl* mutant (**Fig. 2f**). These results strongly suggest that $CO_2$ inhibits
176 accumulation of the *LHCSR3* transcript and that the decline of *LHCSR3* mRNA in WT cells
177 supplemented with acetate is a consequence of the $CO_2$ released as the acetate is metabolized. The

178 extent of this inhibition by acetate-derived $CO_2$ appears to depend mostly on the rate of
179 photosynthetic $CO_2$ fixation (consumption of $CO_2$) because acetate was taken up by WT cells at
180 similar rates under both LL and HL conditions (**Fig. 2c** and **f**). Indeed, under LL conditions, where
181 $CO_2$ fixation is slow, acetate and $CO_2$ repressed *LHCSR3* to the same extent (**Fig. 2a**); under HL
182 conditions, where $CO_2$ fixation is much faster, the effect of acetate on the *LHCSR3* transcript level
183 was much smaller than that of $CO_2$, which was continuously provided in excess (5%) via sparging
184 (**Fig. 2d**).

185 We also employed constraint-based metabolic modelling to assess *in silico* whether acetate
186 metabolism in *Chlamydomonas* leads to an increase in the concentration of intracellular $CO_2$ under
187 different growth conditions (**Supplementary Note 1, Supplementary Fig. 2, Supplementary**
188 **Tables 1-3, Supplementary Datasets 1-3**). The findings from this approach support the hypothesis
189 that there are changes in the internal $CO_2$ concentration under autotrophic and mixotrophic growth
190 conditions at different light intensities. These predicted changes in internal $CO_2$ levels under the
191 different conditions for the WT and mutant cells are congruent with the levels of accumulation of
192 *LHCSR3* transcripts that were measured.
193

194 **CIA5 links HL and low $CO_2$ responses**

195 The responses to HL and low $CO_2$ have been traditionally studied separately, despite several lines
196 of evidence suggesting that they are integrated[26,27,32]. To elucidate the molecular connection
197 between photoprotection and CCM, we analyzed mRNA accumulation of twelve genes implicated
198 as functionally involved in the CCM, previously shown to be strongly expressed under low $CO_2$
199 conditions[33,34] and/or to be under the control of CIA5[26]. Specifically, we analysed twelve CCM-
200 related genes encoding LOW-$CO_2$-INDUCIBLE PROTEIN B (LCIB) and E (LCIE), involved in
201 $CO_2$ uptake; HIGH-LIGHT ACTIVATED 3 (HLA3), LOW $CO_2$-INDUCED 1 (LCI1),
202 CHLOROPLAST CARRIER PROTEIN 1 (CCP1), CCP2, LCIA, BESTROPHINE-LIKE
203 PROTEIN 1 (BST1), acting as Ci transporters; carbonic anhydrases CAH1, CAH3, CAH4; the
204 nuclear regulator LOW-$CO_2$ -STRESS RESPONSE 1 (LCR1).

205 When LL-acclimated, air sparged WT, *icl* and *icl-C* strains were exposed to HL (experiment
206 described in **Fig. 1**) a marked increase (5 to 600-fold) in CCM transcript levels was observed in
207 WT cells (**Supplementary Fig. 3**), in accordance with recent studies[28,32]; this increase was strongly
208 suppressed by $CO_2$ and to a lesser extent by acetate, which did not affect CCM gene expression in
209 the *icl* mutant (**Supplementary Fig. 3**). This pattern of mRNA accumulation was essentially
210 identical to that of *LHCSR3* (**Fig. 1a**), highlighting the tight connection between HL and low-$CO_2$

211 responses in *Chlamydomonas*. The $CO_2$-mediated repression was more pronounced for most of the
212 CCM genes relative to *LHCSR3* (**Fig. 1a** and **c, Supplementary Fig. 3**).

213 CIA5 has been shown to regulate accumulation of transcripts from both the CCM genes[26,27] and
214 *LHCSR3*[28]. To obtain a comprehensive view of the photoprotection capacity of the *cia5* mutant, air
215 sparged WT and *cia5* cells grown in LL were shifted to HL, and the transcript and protein levels
216 from the qE effector genes were monitored. Remarkably, a lack of *CIA5* resulted in much lower
217 accumulation of *LHCSR3* mRNA than in WT cells; 50 times lower at LL and over 200 times lower
218 at HL. This phenotype was fully reversed by ectopic expression of the WT *CIA5* gene (**Fig. 3a)**.
219 *PSBS* also showed a significant CIA5 dependent control at the mRNA level, although at a smaller
220 extent (**Fig. 3a**). The *cia5* mutant accumulated slightly more *LHCSR1* mRNA in both LL and HL
221 (~2 fold), however this phenotype was not restored in the complemented *cia5-C* strain (**Fig. 3a**);
222 we conclude that *LHCSR1* mRNA accumulation is CIA5-independent. We also quantified
223 accumulation of mRNAs of *CAH1* and *LCIA*, which are known to be strongly dependent on
224 CIA5[27,35]. As expected, the *cia5* mutant cells failed to activate either of those genes in HL while
225 their activation was fully restored in the complemented *cia5-C* strain (**Fig. 3a**).

226 At the protein level, no LHCSR3 protein was detected in the *cia5* mutant in either LL or HL **(Fig.**
227 **3b**). We were unable to immunologically detect the PSBS protein under these experimental
228 conditions, in agreement with previous findings showing that PSBS protein accumulation is highly
229 transient in cell cultures bubbled with air[6]. Importantly, the LHCSR1 protein accumulated to high
230 levels in the mutant under both LL (conditions in which no protein is apparent in the WT) and HL
231 conditions; this phenotype was fully reversed by ectopic expression of the WT *CIA5* gene (**Fig. 3b**).
232 This result suggests that CIA5 acts as a suppressor of LHCSR1 translation (and/or decreases protein
233 stability) in both LL and HL. Our data additionally suggest that accumulation of LHCSR1 protein
234 occurs through a compensatory, CIA5-controlled posttranscriptional mechanism that provides
235 photoprotection under conditions in which the cells have almost no LHCSR3 protein (compare
236 LHCSR1 and LHCSR3 immunoblots in **Fig. 3b**). Supporting this idea, the qE levels in *cia5,*
237 although lower than WT and *cia5-C* (**Fig. 3c** and **Supplementary Fig. 4**), they were unexpectedly
238 high considering the absence of LHCSR3 protein (**Fig. 3b**); we attribute this result to
239 overaccumulation of LHCSR1 in this mutant (**Fig. 3b)**. Together, our results demonstrate a key role
240 of CIA5 in regulating photoprotection, activating *LHCSR3* and to a lesser extent *PSBS* transcription
241 and suppressing LHCSR1 protein accumulation.

242

243

244 **CIA5 and $CO_2$ availability regulate LHCSR1 protein stability**

245

246 The high levels of accumulation of LHCSR1 protein in the *cia5* mutant (**Fig. 3b**) suggest that $CO_2$
247 availability could be the key determinant for LHCSR1 protein accumulation, as CIA5 is not
248 functional under high $CO_2$ levels[15-17]. Given the novelty of this finding, we decided to perform
249 additional experiments to provide more details concerning LHCSR1 regulation. LL-acclimated WT
250 cells sparged with air were exposed to HL sparged with air or 5% $CO_2$ and the mRNA and protein
251 levels were quantified over a 25-h period. Upon initial exposure to HL, *LHCSR1* mRNA rapidly
252 increased (2 orders of magnitude in 1 h) and then decreased to the initial level (between 4 and 8 h),
253 in agreement with a previous report[36], in the presence or absence of high $CO_2$ (**Fig. 4a**). In contrast,
254 the presence of high $CO_2$ sustained high levels of LHCSR1 protein over the 25-h incubation period
255 relative to cultures sparged with air (**Fig. 4b**). These results suggest that elevated $CO_2$ either
256 promotes translation of *LHCSR1* mRNA or is involved in stabilizing the protein once it is
257 synthesized. This contrasts with the behaviour of LHCSR3 for which there was a strong correlation
258 between the level of mRNA and protein (the RNA was 3 orders of magnitude lower in 5% $CO_2$ and
259 the protein was no longer detected) (**Fig. 4**). The kinetics of *PSBS* transcript accumulation in HL
260 very much resembled those of *LHCSR1*, with $CO_2$ not having a strong impact on transcript
261 accumulation **(Fig. 4a)**. PSBS protein accumulation was not detectable under the experimental
262 conditions used. Taken together, our data demonstrate the critical importance of CIA5 and $CO_2$ in
263 regulating the different qE effectors, mainly *LHCSR3* and less strongly *PSBS* at the transcript level,
264 and LHCSR1 at the protein level.

265

266 **Intracellular $CO_2$ levels regulate photoprotective and CCM gene expression in the absence of**
267 **light**

268 To de-convolute the light and $CO_2$ signals regulating *LHCSR3*, we exposed the cells to different
269 light intensities and $CO_2$ concentrations (**Supplementary Fig. 5**). High $CO_2$ levels completely
270 abolished accumulation of LHCSR3 protein at all light intensities, in accord with the results of **Fig.**
271 **1b** and **d** and **Fig. 4b**. On the contrary, low $CO_2$ levels led to very high accumulation of LHCSR3
272 protein at 150 and 300 µmol photons $m^{-2}$ $s^{-1}$. Under low $CO_2$, LHCSR3 protein was also detectable
273 even at the very low light intensity of 10 µmol photons $m^{-2}$ $s^{-1}$ **(Supplementary Fig. 5)**, as
274 previously demonstrated[6].

275 Prompted by this result, we tested whether changes in $CO_2$ levels could activate transcription of
276 *LHCSR3* in complete darkness. We shifted air sparged cells to sparging with $CO_2$-free air (Very

277 low CO2; $VLCO_2$) in complete darkness and to our surprise, we observed that despite the absence
278 of light, that a drop in $CO_2$ availability was sufficient to trigger *LHCSR3* mRNA accumulation by
279 ~ 700-fold (**Fig. 5a**), with an increase in accumulation of the protein by 3-fold (**Fig 5b** and **c**;
280 compare WT air with WT $VLCO_2$). In addition, when HL was combined with $VLCO_2$, which is
281 expected to result in an even greater reduction in the intracellular $CO_2$ concentration, the levels of
282 *LHCSR3* mRNA and protein further increased, reaching levels of ~4500-fold (mRNA) and 21-fold
283 (protein) compared to air dark conditions (**Fig. 5a-c**). Interestingly, this light-independent
284 regulation of mRNA accumulation was under the control of CIA5 as accumulation of *LHCSR3*
285 transcripts was abolished in the *cia5* mutant (**Fig. 5a**) and a full reversal of these phenotypes (gene
286 expression and protein levels) was observed in the *cia5-C* strain (**Fig. 5a** and **b**). We also observed
287 significant *LHCSR3* transcript accumulation in the *cia5* mutant when cells were shifted from dark-
288 air to HL-$VLCO_2$, which was however 9-fold lower compared to the WT (**Fig. 5a**), and that was
289 rescued to WT-levels in the *cia5-C* complemented line. This CIA5-independent regulation of
290 mRNA in the presence of light could account for the contribution of light signaling in *LHCSR3*
291 gene expression, possibly via phototropin[10] or via the generation of reactive oxygen species[28].

292 We could observe that *LHCSR1* transcripts were also induced in the dark (shift from dark-air to
293 dark-$VLCO_2$), but this induction was very low (7-fold) and appeared to be CIA5 independent
294 (**Supplementary Fig. 6a**). At the protein level however, LHCSR1 over-accumulated in the *cia5*
295 mutant under all conditions tested (**Supplementary Fig. 6b**), confirming our previous findings
296 (**Fig. 3b)**. *PSBS* also showed a CIA5-dependent dark induction of transcripts (shift from dark-air to
297 dark-$VLCO_2$), although this induction was low (5-fold); complementation with the CIA5 *gene*
298 (*cia5-C* strain) did not rescue the phenotype in dark-air conditions and only partially rescued it
299 under dark-$VLCO_2$ (**Supplementary Fig. 6a** and **b**). Both mRNA and protein accumulation of
300 PSBS accumulated in a CIA5-dependent manner when cells were shifted from dark-air to HL-
301 $VLCO_2$ (**Supplementary Fig. 6a** and **b**); under these conditions the phenotypes were fully reversed
302 in the *cia5-C* strain. This CIA5-dependent regulation of PSBS can most likely explain previously
303 reported findings that PSBS protein accumulation was responsive to $CO_2$ abundance, with its
304 accumulation reaching maximum levels under low $CO_2$ and HL conditions[6].

305 We also measured CCM-related gene expression in the dark. As shown in **Fig. 5a** and
306 **Supplementary Fig. 6a**, high levels of CCM-related transcripts were observed in the dark when
307 the cells experienced $VLCO_2$ conditions (compare "dark air" with "dark $VLCO_2$"). The
308 combination of HL and $VLCO_2$ conditions, either elicited very small (less than two-fold) or no
309 additional increase (compare "HL $VLCO_2$" to "dark $VLCO_2$") in their level of the mRNA

accumulation (**Fig. 5a** and **Supplementary Fig. 6a**). As expected CIA5 was critical for expression of the CCM genes under all conditions tested **(Fig. 5a** and **Supplementary Fig. 6a**).

Our data points out that the LHCSR1 protein overaccumulation in *cia5* was fully reversed only when *cia5-C* cells were pre-acclimated in the light (**Fig. 3b**); when pre-acclimation took place in the dark the phenotype was only partially rescued (**Supplementary Fig. 6b**). The same is true for the mRNA accumulation of *PSBS* (compare LL; **Fig. 3a** with air-dark; **Supplementary Fig. 6a**), *CAH1* (compare LL; **Fig. 3a** with air-dark; **Supplementary Fig. 6a**), *LCIA* (compare LL; **Fig. 3a** with air-dark; **Fig. 5a**), while in the case of LHCSR3 a full reversal of the CIA5-dependent phenotype was seen no matter what pre-acclimation strategy was followed (**Fig. 3a**, **b** and **Fig. 5a, b**). A plausible explanation for these results is the differential accumulation of CIA5 protein in the different acclimation regimes due to the promoter used. In line with this explanation, CIA5 expression in *cia5-C* is driven by the light-inducible promoter of the *PSAD* gene, and, as a result, less CIA5 protein accumulated in the dark-acclimated *cia5-C* compared to the LL-acclimated (**Supplementary Fig. 7a**). This in turn affects the relative abundance of CIA5 available for binding with its target molecules (DNA binding sites or CIA5-interacting proteins), ultimately affecting the reversal of the CIA5-related phenotypes.

Overall, these data challenge the view concerning the regulation of photoprotection and CCM and bring $CO_2$ to the forefront as a crucial signal controlling *LHCSR3* and CCM-related genes induction in the absence of light.

**Link between photosynthetic electron transfer and $CO_2$ intracellular concentration**

Our finding that *LHCSR3* is regulated by light-independent $CO_2$ availability has guided us in revising the way in which we view the impact of photosynthetic electron transfer **(**PET) on LHCSR3 accumulation; i.e. inhibition of LHCSR3 accumulation in photosynthetic mutants or WT cells treated with photosynthetic inhibitors[10,11].

We propose that enhanced PET, occurring under HL conditions, facilitates $CO_2$ fixation, draws down the intracellular $CO_2$ concentration and induces *LHCSR3* transcription. In contrast, when PET is impaired, intracellular $CO_2$ levels increase, thus promoting *LHCSR3* transcript inhibition. In accordance, there is a marked increase of $CO_2$ in cultures treated with DCMU, an inhibitor of photosystem II[37], measured either as dissolved $CO_2$ in the culture medium[38], or as $CO_2$ in the air stream coming from the headspace of the column bioreactor (**Fig. 6a**). In order to test our hypothesis, we analyzed the combined effect of DCMU and $CO_2$ on the accumulation of mRNA

342 from the *LHCSR3* and two CCM genes in WT cultures shaken without or with $VLCO_2$ sparging. In
343 accord with previous reports[10,39], DCMU completely blocked the HL elicited accumulation of
344 *LHCSR3* mRNA; *LHCSR3* mRNA after 1h exposure to HL diminished to ten times lower levels
345 than the initial LL levels (shown as dotted line in graph) (**Fig. 6b**), which most likely reflects
346 degradation of the transcripts following inactivation of the gene after the addition of DCMU.
347 Previous work has shown that *LHCSR3* transcripts are rapidly lost once the gene becomes inactive[10]
348 which has also been observed for the *CAH4* transcript[40]. However, when the cultures were sparged
349 with $VLCO_2$ air, which would result in maintenance of a continuous $VLCO_2$ concentration in the
350 cultures, a large part of the DCMU elicited inhibition was relieved (**Fig. 6b**), supporting the idea
351 that light primarily impacts *LHCSR3* transcript levels by altering $CO_2$ consumption and the
352 intracellular (and/or extracellular) $CO_2$ concentration. In contrast to *LHCSR3*, sparging with
353 $VLCO_2$ only partly relieved the suppression of transcript accumulation for the CCM genes in the
354 presence of DCMU (**Fig. 6b**). This difference may reflect the fact that CCM gene expression is
355 solely regulated by $CO_2$ via CIA5 (**Fig. 5a**) and that sparging with $VLCO_2$ in the presence of DCMU
356 does not reduce the $CO_2$ levels enough to attain full gene activation. It is also possible that longer
357 incubation time with $VLCO_2$ would have relieved a larger part of the DCMU-elicited inhibition of
358 CCM genes (**Fig. 6b**) as implied by the slow kinetics of *CAH4/5* mRNA accumulation when cells
359 are shifted from 5% $CO_2$ to air[40].
360

361 **Discussion**

362

363 In this work, we presented findings that advance our understanding of integration between $CO_2$-
364 and light-dependent signaling in *Chlamydomonas*. We propose that the intracellular level of $CO_2$,
365 defined by the equilibrium between light-driven $CO_2$ fixation in chloroplasts and the generation of
366 $CO_2$ by mitochondrial metabolism (e.g. acetate assimilation), is a key regulator of two major
367 processes in photosynthetic organisms: the CCM and photoprotection (**Fig. 7**).

368 To better understand the role of $CO_2$ in regulating photoprotection and its integration with light, we
369 designed experiments to separate the effects of the two signals (**Fig. 5-7**); we reduced the
370 concentration of $CO_2$ in the microalgae medium by sparging it with $VLCO_2$ in complete darkness.
371 This abrupt change in $CO_2$ levels experienced by the cultures in the dark may be considered a
372 condition only encountered in the laboratory. However, in certain ecological niches, such as soil or
373 catchments with elevated levels of organic matter[33], *Chlamydomonas* would encounter changes in
374 the levels of $CO_2$ that would be dependent on the microbes and the ratio between respiration and

375 photosynthesis in the environment. Our experimental setup allowed us to observe a strong increase
376 of *LHCSR3* transcript levels when cells were shifted from air-$CO_2$ to $VLCO_2$ levels in the dark
377 (**Fig. 5**), a very surprising result as the accumulation of *LHCSR3* mRNA was considered so far to
378 be strictly light-dependent[5,11,39]. Moreover, with this strategy we can disentangle light from $CO_2$
379 signalling effects; while dark induction of *LHCSR3* under $CO_2$-depletion was completely dependent
380 on CIA5, light could still strongly impact expression of all photoprotective genes in the *cia5* mutant,
381 which was not the case for CCM gene expression that was completely abolished in the light or dark
382 in the absence of CIA5 (**Fig. 5** and **Supplementary Fig. 6**). This impact of light on qE gene
383 expression may be the consequence of photoperception (e.g. PHOT1)[10], but also the generation of
384 light-dependent signals such as reactive oxygen species[28]. Furthermore, a CIA5-independent
385 regulation (also observed in **Fig. 3a**) explains *LHCSR3* induction in high $CO_2$-acclimated WT cells
386 (cells in which CIA5 is not functional[15-17]) as they transition from LL to HL (**Fig. 1a**), which was
387 not observed for CCM genes tested under identical conditions (**Supplementary Fig. 3**); it also
388 explains why the $CO_2$-mediated repression was more pronounced for most of the CCM genes
389 relative to LHCSR3 (**Fig. 1a** and **c**, **Supplementary Fig. 3**). $CO_2$ and CIA5 appear to be of
390 paramount importance in signal integration and transduction, regulating expression of both
391 photoprotection and CCM genes. For instance, $CO_2$ represses the UV-B elicited, UVR8-mediated
392 expression of *LHCSR3*, and CIA5 is absolutely required for this expression[28]. Moreover, our results
393 have shown that high $CO_2$ levels or the absence of CIA5 have a severe impact on *LHCSR3* gene
394 expression and, although HL can still induce *LHCSR3* transcription, no protein is detected (**Fig. 1,**
395 **3** and **5**).

396 Besides transcriptionally controlling *LHCSR3*, CIA5 post-transcriptionally controls LHCSR1. Our
397 view on LHCSR1 regulation by light and CIA5 is as follows: under LL conditions, LHCSR1 protein
398 accumulates in *cia5* while it is non-detectable in WT and *cia5-C* (**Fig. 3b**), suggesting that CIA5
399 suppresses LHCSR1 protein accumulation. Exposure to HL triggers a CIA5-independent *LHCSR1*
400 mRNA accumulation (**Fig. 3a**), possibly driven by reactive species, previously shown to favor
401 *LHCSR1* mRNA accumulation[41]. As a result, LHCSR1 protein accumulates in WT and *cia5-C* in
402 HL, despite the fact that suppression of LHCSR1 protein by CIA5 still occurs; indeed, LHCSR1
403 accumulates to higher levels in the *cia5* mutant as compared to WT and *cia5-C* under HL conditions
404 (**Fig. 3b**). In line with the above observations in the *cia5* mutant, high levels of LHCSR1 protein
405 accumulate in WT under high $CO_2$, conditions that inactivate CIA5 (**Fig. 4b**). Put together, our
406 findings unveil a multilevel role of CIA5 in regulating qE; inactivation of CIA5 in high $CO_2$ or by
407 eliminating the CIA5 gene blocks *LHCSR3* transcript accumulation, while it promotes LHCSR1

408 protein accumulation (**Fig. 3** and **4**). Further investigation will be required to explain how a single
409 nuclear factor, CIA5, can control cellular processes happening in different cellular compartments;
410 transcription in the nucleus and translation in the cytosol.

411 Our results provide an interpretation of the findings that PET is required for LHCSR3
412 accumulation[11], activation of the CCM and expression of CCM genes[42]. We propose that $CO_2$,
413 either provided directly or indirectly through metabolic generation, represents a critical link
414 between PET and transcriptional regulation of *LHCSR3* and the CCM genes (**Fig. 6**).
415 Photosynthesis draws down cellular $CO_2$ levels, and therefore, blocking photosynthesis with
416 DCMU leads to the accumulation of $CO_2$ (**Fig. 6a**) which elicits *LHCSR3* repression, while sparging
417 DCMU-treated cells with $VLCO_2$ almost fully derepresses *LHCSR3* (and partially CCM)
418 expression (**Fig. 6b**). DCMU also upregulates genes of the leucine degradation pathway[43] leading
419 to the generation of acetoacetate and acetyl-CoA, which can lead to oxidative $CO_2$ production.
420 Whether leucine itself has a regulatory role or $CO_2$ is the key regulator deserves further attention.
421 It is tempting to propose that $CO_2$ is a retrograde signal that readily diffuses through the cell and
422 impacts nuclear gene expression, which would integrate both mitochondrial and chloroplastic
423 metabolic activities.

424 The way in which *Chlamydomonas* senses $CO_2$ is not clear. Our data, i.e. accumulation of *LHCSR3*
425 and CCM genes in the dark, exclude the possibility that a metabolite produced by photorespiration
426 plays a major signalling role, as previously proposed [44]. $CO_2$ itself might also serve as the metabolite
427 being recognized by a putative sensor that could be controlled by carbamylation, a $CO_2$-mediated
428 post-translational modification that regulates, among others, the activation of Rubisco[45].
429 Furthermore, the large number of adenosine and guanylyl cyclases in *Chlamydomonas*[46] suggests
430 that cyclic nucleotides play an important role in controlling various processes in this alga; these
431 metabolites have been shown to be involved in mating[47], regulation of flagellar beating and
432 phototaxis[48-50], in regulating inorganic nitrogen assimilation[51] and in restoring LHCSR3
433 accumulation in the absence of phototropin[10]. Cyclases have been shown to act as $CO_2$ sensors (as
434 bicarbonate) in mammalian cells[52], making it plausible that they can also serve as sensors in
435 *Chlamydomonas*. As cyclic nucleotide signalling and calcium are tightly linked[52], we anticipate an
436 important role for calcium in $CO_2$ sensing; calcium signalling has already been shown to be
437 involved in the regulation of both *LHCSR3* and CCM genes[11,53].

438 Overall, our work shows that the intracellular $CO_2$ level is the main factor in regulating CCM genes
439 and *LHCSR3* in *Chlamydomonas* (**Fig. 7**). Exposure to HL increases the $CO_2$ fixation rate which
440 causes a drop in intracellular $CO_2$ which, in turn, actives both photoprotection- and CCM-related

441 genes. Depletion of $CO_2$ is sufficient to drive high expression levels of CCM genes and *LHCSR3*
442 even in complete darkness. On the other hand, high $CO_2$ levels, either generated through enhanced
443 respiratory activity or impaired photosynthetic electron transport, repress *LHCSR3* and CCM genes
444 while at the same time stabilizing the LHCSR1 protein, which likely acts as a backup
445 photoprotection protein under conditions where LHCSR3 is not expressed. Furthermore, our data
446 reveals a closer interconnection of photoprotection and CCM as CIA5, the CCM master regulator,
447 also exerts control over *LHCSR3* and to a lesser extent over *PSBS* mRNA levels, while repressing
448 LHCSR1 protein accumulation. Our findings highlight the need to develop an integrated approach
449 that examines the role of $CO_2$ and light, not only as substrates of photosynthetic $CO_2$ fixation, but
450 also as signals regulating photoprotection, CCM, and at a wider context genome-wide gene
451 expression.
452
453
454
455

456 **Methods**

457 **Chemicals**

458 DCMU (3-(3,4-dichlorophenyl)-1,1-dimethylurea) was purchased from Sigma. Stock solutions of
459 DCMU were prepared in ethanol (40 mM).

460

461 **Strains and conditions**

462 *Chlamydomonas* strains were grown under 20 µmol photons $m^{-2}$ $s^{-1}$ in Tris-acetate-phosphate (TAP)
463 medium [54] at 23 ºC in Erlenmeyer flasks shaken at 125 rpm. For all experiments cells were
464 transferred to Sueoka's High Salt medium[55] supplemented when needed with 10 mM sodium
465 acetate, at 2 million cells $mL^{-1}$ in 80 mL capacity columns, unless otherwise stated, sparged with
466 air, air enriched with 5% $CO_2$, or very low $CO_2$ air ($VLCO_2$; generated by passing the air through
467 soda lime) and exposed to light intensities as described in the text and figure legends.
468 *Chlamydomonas* strain 137c mt+ was used as WT. The *icl* (defective in *ICL1*; gene ID:
469 Cre06.g282800), *icl-C* (*icl* strain complemented with the WT *ICL* gene), *dum11* (defective in
470 defective in ubiquinol cytochrome c oxidoreductase of the respiratory complex III; geneID:
471 CreMt.g000300) and *cia5* (defective in *CIA5*, aka CCM1; geneID: Cre02.g096300;
472 Chlamydomonas Resource Centre strain CC-2702) mutants were previously generated [15,21,29]. For
473 complementation of *cia5*, a 3.5-kbp genomic DNA fragment from CC-125 containing
474 the *CIA5* coding region was amplified by PCR using Platinum™ SuperFi™ DNA Polymerase
475 (Thermo Fisher Scientific) and primers gib-cia5-fw and gib-cia5-rev (**Supplementary Table 4**),
476 gel purified and cloned into pLM005 [56] by Gibson assembly [57] for expression under control of
477 the *PSAD* promoter. Junctions and insertion were sequenced, and constructs were linearized by
478 EcoRV before transformation into *cia5*. Eleven ng/kb of linearized plasmid [56] mixed with 400 µL
479 of 1.0 x$10^7$ cells $mL^{-1}$ were electroporated in a volume of 120 mL in a 2-mm-gap electro cuvette
480 using a NEPA21 square-pulse electroporator (NEPAGENE, Japan). The electroporation parameters
481 were set as follows: Poring Pulse (300V; 8 ms length; 50 ms interval; one pulse; 40% decay rate; +
482 Polarity), Transfer Pulse (20V; 50 ms length; 50 ms interval; five pulses; 40% decay rate; +/-
483 Polarity). Transformants were plated onto solid agar medium containing 10 µg/ml paromomycin
484 and screened for fluorescence using a Tecan fluorescence microplate reader (Tecan Group Ltd.,
485 Switzerland). Parameters used were as follows: YFP (excitation 515/12 nm and emission 550/12
486 nm) and chlorophyll (excitation 440/9 nm and 680/20 nm). Transformants showing a high
487 YFP/chlorophyll ratio were further analyzed by immunoblotting using anti-FLAG antibodies
488 (**Supplementary Fig. 7b**). Among the transformants analyzed the *cia5-C-a1* (*cia5-C* throughout

489 the text) was retained for further analyses in the present study, after verifying that it grows similarly
490 with the WT under phototrophic conditions on agar (**Supplementary Fig. 7c**). Unless otherwise
491 stated, LL conditions corresponded to 20 µmol photons $m^{-2}$ $s^{-1}$ while HL conditions corresponded
492 to 600 µmol photons $m^{-2}$ $s^{-1}$ of white light (Neptune L.E.D., France; see **Supplementary Fig. 8** for
493 light spectrum). All experiments were repeated three times to examine reproducibility, unless
494 otherwise stated.
495

496 **Light acclimation experiments**

497 Cells were acclimated overnight in High Salt Medium (HSM) in LL sparged with air, in the presence
498 or absence of acetate, or sparged with 5% $CO_2$. Following this acclimation period, cells were
499 transferred from LL to HL, with all other conditions identical to those of the acclimation period.
500 Samples were collected after 1 h for RNA analyses and after 4 h for protein analysis and
501 measurements of photosynthetic activity.
502

503 **Fluorescence-based measurements**

504 Fluorescence-based photosynthetic parameters were measured with a a pulse modulated amplitude
505 fluorimeter (MAXI-IMAGING-PAM, HeinzWaltz GmbH, Germany). Prior to the onset of the
506 measurements, cells were acclimated to darkness for 15 min. Chlorophyll fluorescence was
507 recorded under different intensities of actinic light; starting with measurements in the dark
508 (indicated as D below the x-axis of the graphs), followed by measurements at 21 µmol photons $m^{-2}$
509 $s^{-1}$ (indicated as L1 below the x-axis of the graphs) and 336 µmol photons $m^{-2}$ $s^{-1}$ (indicated as L2
510 below the x-axis of the graphs) and finishing with measurements of fluorescence relaxation in the
511 dark. The calculations of the different photosynthetic parameter was performed based on[58] as
512 follows: The relative photosynthetic electron transfer rate (rETR) was calculated as $(F\mathrm{m}' - F)/F\mathrm{m}'$
513 $\times$ I; $F$ and $F\mathrm{m}'$ are the fluorescence yield in steady state light and after a saturating pulse in the
514 actinic light, respectively; $I$ is the light irradiance in µmol photons $m^{-2}$ $s^{-1}$; NPQ was calculated as
515 $(F\mathrm{m} - F\mathrm{m}')/F\mathrm{m}'$; $F\mathrm{m}$ is the maximal fluorescence yield in dark-adapted cells; the effective
516 photochemical quantum yield of photosystem II was calculated as Y(II) = (Fm'-F)/Fm'; qE was
517 estimated as the fraction of NPQ that is rapidly inducible in the light and reversible in the dark.
518

519 **mRNA quantification**

520 Total RNA was extracted using the RNeasy Mini Kit (Qiagen) and treated with the RNase-Free
521 DNase Set (Qiagen). 1 µg total RNA was reverse transcribed with oligo dT using Sensifast cDNA

522 Synthesis kit (Meridian Bioscience, USA). qPCR reactions were performed and quantitated in a
523 Bio-Rad CFX96 system using SsoAdvanced Universal SYBR Green Supermix (BioRad). The
524 primers (0.3 µM) used for qPCR are listed in **Supplementary Table 4**. A gene encoding G protein
525 subunit-like protein (GBLP)[59] was used as the endogenous control, and relative expression values
526 relative to *GBLP* were calculated from three biological replicates, each of which contained three
527 technical replicates.
528

529 **$CO_2$ measurements**

530 $CO_2$ concentration was measured in the air stream coming from the headspace of a HSM or culture
531 containing column using the $CO_2$ Probe GMP251 connected to the MI70 data logger from Vaisala
532 (Vantaa, Finland).
533

534 **Immunoblotting**

535 Protein samples of whole cell extracts (0.5 µg chlorophyll or 10 µg protein) were loaded on 4-20%
536 SDS-PAGE gels (Mini-PROTEAN TGX Precast Protein Gels, Bio-Rad) and blotted
537 onto nitrocellulose membranes. Antisera against LHCSR1 (AS14 2819, 1:15000 dilution),
538 LHCSR3 (AS14 2766, 1:15000 dilution), ATPB (AS05 085, 1:15000 dilution) were from Agrisera
539 (Vännäs, Sweden); previously described was antisera against *C. reinhardtii* PSBS [6] (used at a
540 dilution of 1:1000). ATPB was used as a loading control. An anti-rabbit horseradish peroxidase–
541 conjugated antiserum was used for detection at 1:10000 dilution. Mouse monoclonal antibody
542 against FLAG was purchased from Sigma-Aldrich (F3165, St. Louis, MO, USA) and was used at
543 a dilution of 1:15000. An anti-mouse horseradish peroxidase conjugated antiserum (Jackson
544 Immuno Research Europe LTD) was used as a secondary antibody for 3xFLAG immunoblotting
545 (1:10000 dilution). The blots were developed with ECL detection reagent, and images of the blots
546 were obtained using a CCD imager (ChemiDoc MP System, Bio-Rad). For the densitometric
547 quantification, data were normalized with ATPB.
548

549 **Statistical analyses**

550 Statistical methods were not used to predetermine the sample size. The experiments were not
551 randomized, and the investigators were not blinded to allocation during experimental procedures
552 and data assessment. All statistical tests were performed using the computing environment Prism 9
553 (Graphpad Software, LLC), at a significance level of 0.05. In order to conform mRNA
554 accumulation data to the distributional assumptions of Analysis of Variance (ANOVA), i.e. the

residuals should be normally distributed and variances should be equal among groups, two-way ANOVA was performed with log-transformed data Y=logX where X is mRNA accumulation [60].

**Data availability**

The source data underlying Figures 1-6 and Supplementary Figures 1, 3, 4, 6, 7 are provided as a Source Data file. The Source Data file also includes the exact p-values for figures 1a, 1c, 2a, 2b, 2d, 2e, 3a, 3c, 4a, 5a, and Supplementary figures 1a-b, 3, 6a. All biological material described in this study is available upon request.

**References**


1. Li, Z., Wakao, S., Fischer, B. B. & Niyogi, K. K. Sensing and responding to excess light. *Annu. Rev. Plant Biol.* **60,** 239–260 (2009).
2. Bennett, D. I. G. *et al.* Models and mechanisms of the rapidly reversible regulation of photosynthetic light harvesting. *Open Biol* **9,** 190043 (2019).
3. Alboresi, A., Gerotto, C., Giacometti, G. M., Bassi, R. & Morosinotto, T. Physcomitrella patens mutants affected on heat dissipation clarify the evolution of photoprotection mechanisms upon land colonization. *Proc. Natl. Acad. Sci. U.S.A.* **107,** 11128–11133 (2010).
4. Niyogi, K. K. & Truong, T. B. Evolution of flexible non-photochemical quenching mechanisms that regulate light harvesting in oxygenic photosynthesis. *Curr. Opin. Plant Biol.* **16,** 307–314 (2013).
5. Peers, G. *et al.* An ancient light-harvesting protein is critical for the regulation of algal photosynthesis. *Nature* **462,** 518–521 (2009).
6. Correa-Galvis, V. *et al.* Photosystem II Subunit PsbS Is Involved in the Induction of LHCSR Protein-dependent Energy Dissipation in Chlamydomonas reinhardtii. *J. Biol. Chem.* **291,** 17478–17487 (2016).
7. Tibiletti, T., Auroy, P., Peltier, G. & Caffarri, S. Chlamydomonas reinhardtii PsbS Protein Is Functional and Accumulates Rapidly and Transiently under High Light. *Plant Physiol.* **171,** 2717–2730 (2016).
8. Allorent, G. *et al.* UV-B photoreceptor-mediated protection of the photosynthetic machinery in Chlamydomonas reinhardtii. *Proc. Natl. Acad. Sci. U.S.A.* **113,** 14864–14869 (2016).
9. Dinc, E. *et al.* LHCSR1 induces a fast and reversible pH-dependent fluorescence quenching in LHCII in Chlamydomonas reinhardtii cells. *Proc. Natl. Acad. Sci. U.S.A.* **113,** 7673–7678 (2016).
10. Petroutsos, D. *et al.* A blue-light photoreceptor mediates the feedback regulation of photosynthesis. *Nature* **537,** 563–566 (2016).
11. Petroutsos, D. *et al.* The chloroplast calcium sensor CAS is required for photoacclimation in *Chlamydomonas reinhardtii*. *Plant Cell* **23,** 2950–2963 (2011).
12. Tokutsu, R., Fujimura-Kamada, K., Matsuo, T., Yamasaki, T. & Minagawa, J. The CONSTANS flowering complex controls the protective response of photosynthesis in the green alga Chlamydomonas. *Nat Comms* **10,** 655–10 (2019).
13. Gabilly, S. T. *et al.* Regulation of photoprotection gene expression in Chlamydomonas by a putative E3 ubiquitin ligase complex and a homolog of CONSTANS. *Proc. Natl. Acad. Sci. U.S.A.* **116,** 17556–17562 (2019).

599 14. Maberly, S. C. & Gontero, B. Ecological imperatives for aquatic CO2-concentrating
600 mechanisms. *J. Exp. Bot.* **68,** 3797–3814 (2017).
601 15. Moroney, J. V. *et al.* Isolation and Characterization of a Mutant of Chlamydomonas
602 reinhardtii Deficient in the CO2 Concentrating Mechanism. *Plant Physiol.* **89,** 897–903
603 (1989).
604 16. Fukuzawa, H. *et al.* Ccm1, a regulatory gene controlling the induction of a carbon-
605 concentrating mechanism in Chlamydomonas reinhardtii by sensing CO2 availability.
606 *Proc. Natl. Acad. Sci. U.S.A.* **98,** 5347–5352 (2001).
607 17. Xiang, Y., Zhang, J. & Weeks, D. P. The Cia5 gene controls formation of the carbon
608 concentrating mechanism in Chlamydomonas reinhardtii. *Proc. Natl. Acad. Sci. U.S.A.* **98,**
609 5341–5346 (2001).
610 18. Harris, E. H. Chlamydomonas as a Model Organism. *Annu. Rev. Plant. Physiol.* (2001).
611 doi:10.1146/annurev.arplant.52.1.363
612 19. Wolfe, A. J. The acetate switch. *Microbiol. Mol. Biol. Rev.* **69,** 12–50 (2005).
613 20. Kornberg, H. L. & Krebs, H. A. *Synthesis of cell constituents from C2-units by a modified*
614 *tricarboxylic acid cycle. Nature* **179,** 988–991 (Nature, 1957).
615 21. Plancke, C. *et al.* Lack of isocitrate lyase in Chlamydomonas leads to changes in carbon
616 metabolism and in the response to oxidative stress under mixotrophic growth. *Plant J.* **77,**
617 404–417 (2014).
618 22. Salinas, T., Larosa, V., Cardol, P., Marechal-Drouard, L. & Remacle, C. Respiratory-
619 deficient mutants of the unicellular green alga Chlamydomonas: A review. *Biochimie*
620 (2013). doi:10.1016/j.biochi.2013.10.006
621 23. Fett, J. P. & Coleman, J. R. Regulation of Periplasmic Carbonic Anhydrase Expression in
622 Chlamydomonas reinhardtii by Acetate and pH. *Plant Physiol.* **106,** 103–108 (1994).
623 24. Moroney, J. V., Kitayama, M., Togasaki, R. K. & Tolbert, N. E. Evidence for Inorganic
624 Carbon Transport by Intact Chloroplasts of Chlamydomonas reinhardtii. *Plant Physiol.* **83,**
625 460–463 (1987).
626 25. Polukhina, I., Fristedt, R., Dinc, E., Cardol, P. & Croce, R. Carbon supply and
627 photoacclimation crosstalk in the green alga Chlamydomonas reinhardtii. *Plant Physiol.*
628 1494–1505 (2016). doi:10.1104/pp.16.01310
629 26. Fang, W. *et al.* Transcriptome-wide changes in Chlamydomonas reinhardtii gene
630 expression regulated by carbon dioxide and the CO2-concentrating mechanism regulator
631 CIA5/CCM1. *Plant Cell* **24,** 1876–1893 (2012).
632 27. Miura, K. *et al.* Expression profiling-based identification of CO2-responsive genes
633 regulated by CCM1 controlling a carbon-concentrating mechanism in Chlamydomonas
634 reinhardtii. *Plant Physiol.* **135,** 1595–1607 (2004).
635 28. Redekop, P. *et al.* Transcriptional regulation of photoprotection in dark-to-light transition-
636 more than just a matter of excess light energy. *Sci Adv* (2022).
637 29. Colin, M. *et al.* Mutations affecting the mitochondrial genes encoding the cytochrome
638 oxidase subunit I and apocytochrome b of Chlamydomonas reinhardtii. *Molec. Gen. Genet.*
639 **249,** 179–184 (1995).
640 30. Hanawa, Y., Watanabe, M., Karatsu, Y., Fukuzawa, H. & Shiraiwa, Y. Induction of a high-
641 CO2-inducible, periplasmic protein, H43, and its application as a high-CO2-responsive
642 marker for study of the high-CO2-sensing mechanism in Chlamydomonas reinhardtii.
643 *Plant Cell Physiol.* **48,** 299–309 (2007).
644 31. Soupene, E. *et al.* Rhesus expression in a green alga is regulated by CO(2). *Proc. Natl.*
645 *Acad. Sci. U.S.A.* **99,** 7769–7773 (2002).
646 32. Scholz, M. *et al.* Light-dependent N-terminal phosphorylation of LHCSR3 and LHCB4 are
647 interlinked in Chlamydomonas reinhardtii. *Plant J.* **99,** 877–894 (2019).

648 33. Wang, Y., Stessman, D. J. & Spalding, M. H. The CO2 concentrating mechanism and
649 photosynthetic carbon assimilation in limiting CO2 : how Chlamydomonas works against
650 the gradient. *Plant J.* **82,** 429–448 (2015).
651 34. Mukherjee, A. *et al.* Thylakoid localized bestrophin-like proteins are essential for the CO2
652 concentrating mechanism of Chlamydomonas reinhardtii. *Proc. Natl. Acad. Sci. U.S.A.*
653 **116,** 16915–16920 (2019).
654 35. Yoshioka, S. *et al.* The novel Myb transcription factor LCR1 regulates the CO2-responsive
655 gene Cah1, encoding a periplasmic carbonic anhydrase in Chlamydomonas reinhardtii.
656 *Plant Cell* **16,** 1466–1477 (2004).
657 36. Aihara, Y., Fujimura-Kamada, K., Yamasaki, T. & Minagawa, J. Algal photoprotection is
658 regulated by the E3 ligase CUL4-DDB1DET1. *Nature Plants* **5,** 34–40 (2019).
659 37. Trebst, A. Inhibitors in the functional dissection of the photosynthetic electron transport
660 system. *Photosyn. Res.* **92,** 217–224 (2007).
661 38. Hanawa, Y., Watanabe, M., Karatsu, Y., Fukuzawa, H. & Shiraiwa, Y. Induction of a high-
662 CO2-inducible, periplasmic protein, H43, and its application as a high-CO2-responsive
663 marker for study of the high-CO2-sensing mechanism in Chlamydomonas reinhardtii.
664 *Plant Cell Physiol.* **48,** 299–309 (2007).
665 39. Maruyama, S., Tokutsu, R. & Minagawa, J. Transcriptional regulation of the stress-
666 responsive light harvesting complex genes in *Chlamydomonas reinhardtii*. *Plant Cell*
667 *Physiol.* **55,** 1304–1310 (2014).
668 40. Eriksson, M., Villand, P., Gardeström, P. & Samuelsson, G. Induction and Regulation of
669 Expression of a Low-CO2-Induced Mitochondrial Carbonic Anhydrase inChlamydomonas
670 reinhardtii. *Plant Physiol.* **116,** 637–641 (1998).
671 41. Roach, T., Na, C. S., Stöggl, W. & Krieger-Liszkay, A. The non-photochemical quenching
672 protein LHCSR3 prevents oxygen-dependent photoinhibition in Chlamydomonas
673 reinhardtii. *J. Exp. Bot.* **71,** 2650–2660 (2020).
674 42. Spalding, M. H. in *The molecular Biology of Chloroplasts and Mitochondria in*
675 *Chlamydomonas* (eds. Rochaix, J. D., Goldschmidt-Clermont, M. & Merchant, S. S.)
676 (1998).
677 43. Hemschemeier, A. *et al.* COPPER RESPONSE REGULATOR1-dependent and -
678 independent responses of the Chlamydomonas reinhardtii transcriptome to dark anoxia.
679 *Plant Cell* **25,** 3186–3211 (2013).
680 44. Santhanagopalan, I., Wong, R., Mathur, T. & Griffiths, H. Orchestral manoeuvres in the
681 light: crosstalk needed for regulation of the Chlamydomonas carbon concentration
682 mechanism. *J. Exp. Bot.* **72,** 4604–4624 (2021).
683 45. Linthwaite, V. L. *et al.* The identification of carbon dioxide mediated protein post-
684 translational modifications. *Nat Comms* **9,** 3092 (2018).
685 46. Merchant, S. S. *et al.* The Chlamydomonas genome reveals the evolution of key animal
686 and plant functions. *Science* **318,** 245–250 (2007).
687 47. Hasegawa, E., Hayashi, H., Asakura, S. & Kamiya, R. Stimulation of in vitro motility of
688 Chlamydomonas axonemes by inhibition of cAMP-dependent phosphorylation. *Cell Motil.*
689 *Cytoskeleton* **8,** 302–311 (1987).
690 48. Pasquale, S. M. & Goodenough, U. W. Cyclic AMP functions as a primary sexual signal in
691 gametes of Chlamydomonas reinhardtii. *J. Cell Biol.* **105,** 2279–2292 (1987).
692 49. Gaillard, A. R., Fox, L. A., Rhea, J. M., Craige, B. & Sale, W. S. Disruption of the A-
693 kinase anchoring domain in flagellar radial spoke protein 3 results in unregulated axonemal
694 cAMP-dependent protein kinase activity and abnormal flagellar motility. *Mol. Biol. Cell*
695 **17,** 2626–2635 (2006).

50. Boonyareth, M., Saranak, J., Pinthong, D., Sanvarinda, Y. & Foster, K. W. Roles of cyclic AMP in regulation of phototaxis in *Chlamydomonas reinhardtii*. *Biologia* **64,** 1058–1065 (2009).
51. de Montaigu, A., Sanz-Luque, E., Galván, A. & Fernández, E. A soluble guanylate cyclase mediates negative signaling by ammonium on expression of nitrate reductase in Chlamydomonas. *Plant Cell* **22,** 1532–1548 (2010).
52. Beavo, J. A. & Brunton, L. L. Cyclic nucleotide research -- still expanding after half a century. *Nature* **3,** 710–718 (2002).
53. Wang, L. *et al.* Chloroplast-mediated regulation of CO2-concentrating mechanism by Ca2+-binding protein CAS in the green alga Chlamydomonas reinhardtii. *Proc. Natl. Acad. Sci. U.S.A.* **113,** 12586–12591 (2016).
54. Gorman, D. S. & Levine, R. P. Cytochrome f and plastocyanin: their sequence in the photosynthetic electron transport chain of *Chlamydomonas reinhardii*. *Proc. Natl. Acad. Sci. U.S.A.* **54,** 1665–1669 (1965).
55. Sueoka, N. Mitotic replication of deoxyribonucleic acid in *Chlamydomonas reinhardii*. *Proc. Natl. Acad. Sci. U.S.A.* **46,** 83–91 (1960).
56. Mackinder, L. C. M. *et al.* A repeat protein links Rubisco to form the eukaryotic carbon-concentrating organelle. *Proc. Natl. Acad. Sci. U.S.A.* **113,** 5958–5963 (2016).
57. Gibson, D. G. *et al.* Enzymatic assembly of DNA molecules up to several hundred kilobases. *Nat. Methods* **6,** 343–345 (2009).
58. Genty, B., Briantais, J.-M. & Baker, N. R. The relationship between the quantum yield of photosynthetic electron transport and quenching of chlorophyll fluorescence. *Biochimica et Biophysica Acta (BBA)* **990,** 87–92 (1989).
59. Schloss, J. A. A Chlamydomonas gene encodes a G protein beta subunit-like polypeptide. *Molec. Gen. Genet.* **221,** 443–452 (1990).
60. Schlesselman, J. J. Data Transformation in Two-Way Analysis of Variance. *Journal of the American Statistical Association* (2012). doi:10.1080/01621459.1973.10482435

## Acknowledgments

We are grateful to Dr. Konomi Fujimura-Kamada for performing experiments to validate the dark induction of LHCSR3 in the Minagawa lab; to Claire Remacle for sharing the *icl* and *icl-C* strains and Pierre Cardol for the *dum11* strain. We thank Eric Soupene for valuable insights in the RHP1 induction conditions. We thank Dimitra Karageorgou for performing preliminary experiments in the project and Gilles Curien for fruitful discussions on aspects of microalgae metabolism. We would like to thank the following agencies for funding: The Human Frontiers Science Program through the funding of the project RGP0046/2018 (DP, ARG, PR, ES-L, ZN, AK); the French National Research Agency in the framework of the Young Investigators program ANR-18-CE20-0006 through the funding of the project MetaboLight (DP); the French National Research Agency through the funding of the Grenoble Alliance for Integrated Structural & Cell Biology GRAL project ANR-17-EURE-0003 (DP, MAR-S, GV, YY); the French National Research Agency in the framework of the Investissements d'Avenir program ANR-15-IDEX-02, through the funding of the "Origin of Life" project of the Univ. Grenoble-Alpes (DP, YY) ; the Prestige Marie-Curie

co-financing grant PRESTIGE-2017-1-0028 (MAR-S); the International Max Planck Research School "Primary Metabolism and Plant Growth" at the Max Planck Institute of Molecular Plant Physiology (MA, ZN); the European Union's Horizon 2020 research and innovation program under the Marie Sklodowska-Curie grant agreement no. 751039 (ES-L); the program 'Plan Propio UCO' from University of Cordoba, Spain for postdoctoral Support (ES-L); the Carnegie Institution for Science and the Department of Energy, DE-SC0019417 (ARG); the Marie Curie Initial Training Network Accliphot FP7-PEPOPLE-2012-ITN; 316427 (SF, GF, DP); the Japan Society for the Promotion of Science, JSPS, for the grants-in-Aid for Scientific Research, KAKENHI, 21H04778 and 21H05040 (JM) and the German Research Foundation DFG HI 739/9.2 (MH).

**Author contributions:**

Conceptualization: MAR-S, ES-L, PR, MH, ZN, JM, ARG, DP
Methodology: MAR-S, YY, GV, PR, ES-L, ZN, DP
Investigation: MAR-S, SF, YY, GV, RT, AK, AT, GK, GA, MA, FI
Supervision: GF, ZN, JM, ARG, DP
Writing—original draft: MAR-S, DP
Writing—review & editing: all authors

**Competing interests**

Authors declare that they have no competing interests.

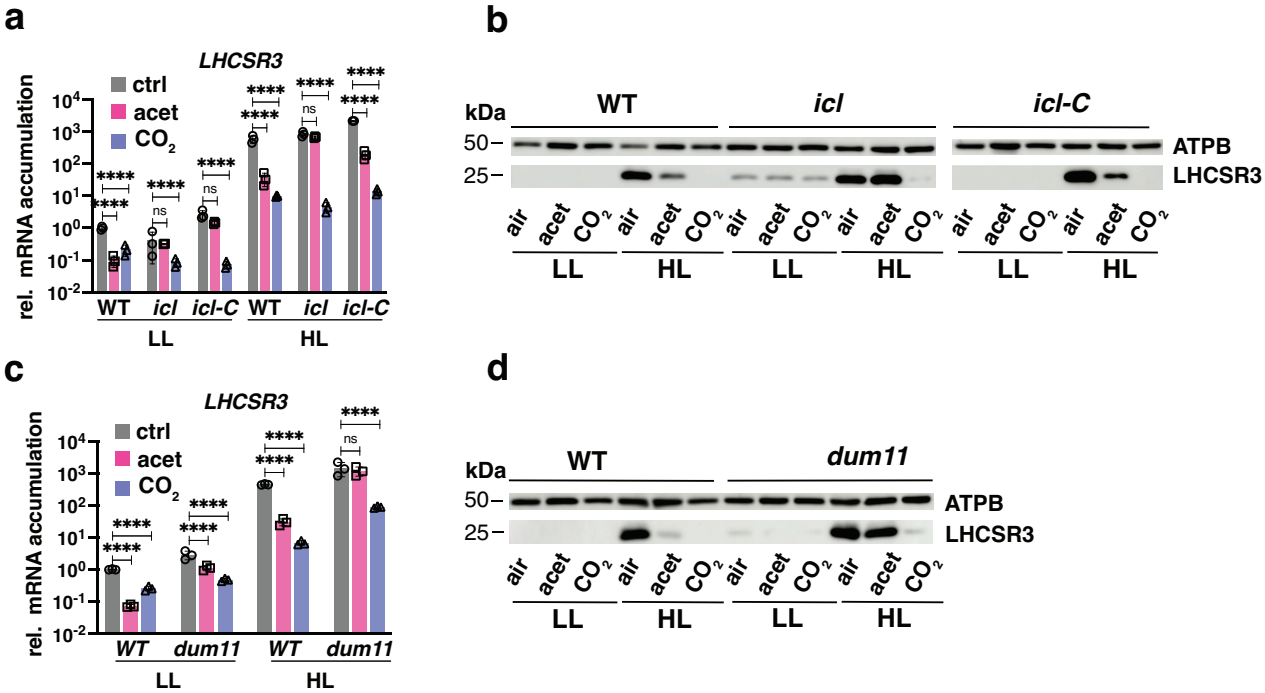


**Figure 1: Acetate needs to be metabolized to inhibit LHCSR3 accumulation**. WT, *icl*, *icl-C* and *dum11* strains were acclimated for 16 h in LL (15 µmol photons $m^{-2}$ $s^{-1}$) in HSM; sparged with air (labelled as "air"); sparged with air and supplemented with 10 mM sodium acetate (labelled as "acet"); sparged with air enriched with 5% $CO_2$ (labelled as "$CO_2$"). After sampling for the LL conditions, light intensity was increased to 600 µmol photons $m^{-2}$ $s^{-1}$ (HL); samples were taken 1 h (RNA) or 4 h (protein) after exposure to HL. **a**, **c**. Accumulation of *LHCSR3* mRNA at the indicated conditions normalized to WT LL ctrl ($n$ = 3 biological samples, mean ± s.d.). The p-values for the comparisons of acetate and $CO_2$ conditions to air are based on ANOVA Dunnett's multiple comparisons test of log10 transformed mRNA data as indicated in the graphs (*, P < 0.005, **, P < 0.01, ***, P < 0.001, ****, P < 0.0001, ns, not significant). Exact p-values can be found at the Source Data file. **b**, **d**. Immunoblot analyses of LHCSR3 and ATPB (loading control) under the indicated conditions. Representative datasets of experiments repeated three times.

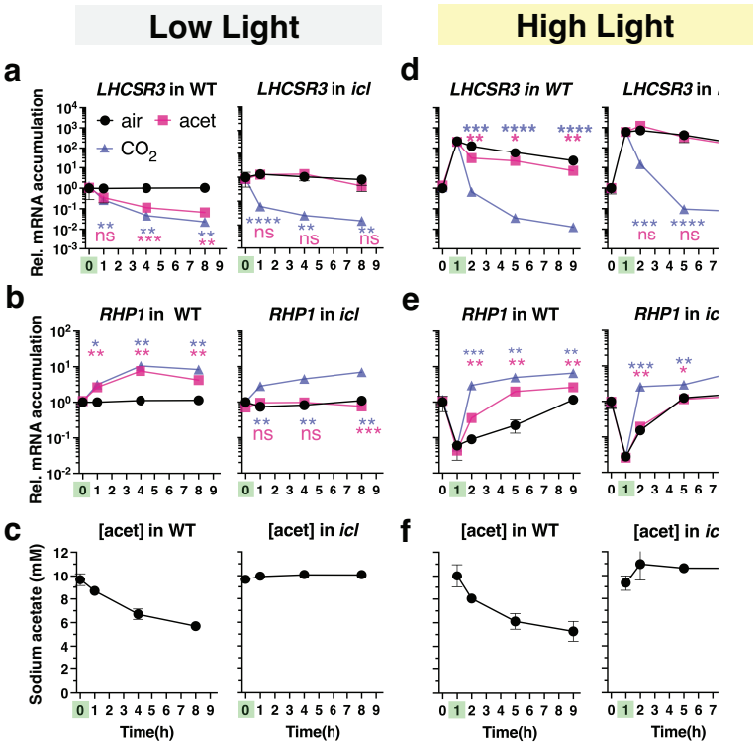


**Figure 2: LHCSR3 inhibition is driven by $CO_2$ derived from the metabolism of acetate.**
**Experiment at LL: a**, **b** mRNA accumulation of *LHCSR3* and *RHP1* and **c** concentration of sodium acetate in the growth medium in WT and *icl* strains. Cells were acclimated overnight at LL (15 µmol photons $m^{-2}$ $s^{-1}$) in HSM sparged with air. At t=0 cells either continued being sparged with air (labelled "air"); or sparged with air and supplemented with 10 mM sodium acetate (labelled "acet"); or sparged with air enriched with 5% $CO_2$ (labelled "$CO_2$"). The addition of acetate or $CO_2$ is indicated with a green mark on the x-axis. Samples were taken at t= 0, 1h, 4h and 8h.
**Experiment at HL: d**, **e** mRNA accumulation of *LHCSR3* and *RHP1* and **f** concentration of sodium acetate in the growth medium in WT and *icl* strains. Cells were acclimated overnight at LL (15 µmol photons $m^{-2}$ $s^{-1}$) in HSM sparged with air; at t=0 light intensity was increased to 600 µmol photons $m^{-2}$ $s^{-1}$. At t=1h cells either continued being sparged with air (labelled "air"); or sparged with air and supplemented with 10 mM sodium acetate (labelled "acet"); or bubbled with air enriched with 5% $CO_2$ (labelled "$CO_2$"), always at 600 µmol photons $m^{-2}$ $s^{-1}$. The time of addition of acetate or $CO_2$ is highlighted in green on the x-axis. Samples were taken at t= 0, 1h, 2h, 5h and 9h. ($n$ = 3 biological samples, mean ± s.d.). The p-values for the comparisons of acetate and $CO_2$ conditions to air (LL; t = 1, 4, 8h, HL; t = 2, 5, 9h) are based on ANOVA Dunnett's multiple comparisons test of log10 transformed mRNA data as indicated in the graphs (*, P < 0.005, **, P < 0.01, ***, P < 0.001, ****, P < 0.0001, ns, not significant), following the color-code of the datasets. Exact p-values can be found at the Source Data file. Please note that in some cases the error bars are smaller than the data point symbols.

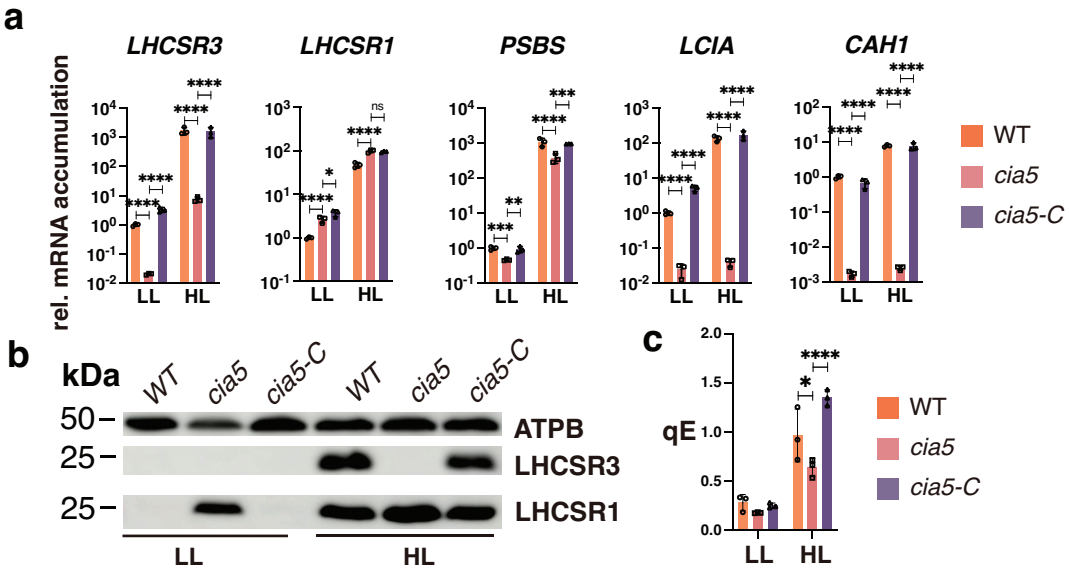


**Figure 3: Cross-talk of responses to HL and low-$CO_2$.**
**a** CC-125 WT, *cia5* and *cia5*-c strains were acclimated for 16 h in LL (15 µmol photons $m^{-2}$ $s^{-1}$) in HSM bubbled with air (labelled as "LL"); after sampling for the LL conditions, light intensity was increased to 600 µmol photons $m^{-2}$ $s^{-1}$ (HL); samples were taken after 1h (RNA) and 4h (protein and photosynthesis measurements). Accumulation of mRNA of genes at the indicated conditions were normalized to WT LL ctrl. ($n$ = 3 biological samples, mean ± s.d.). The p-values for the comparisons of WT with *cia5* and *cia5* with *cia5-C* are based on ANOVA Dunnett's multiple comparisons test of log10 transformed mRNA data as indicated in the graphs. **b** Immunoblot analyses of LHCSR3, LHCSR1 and ATPB (loading control) under the indicated conditions; PSBS was non-detectable at these experimental conditions. Representative dataset of experiment repeated three times. **c** qE of WT, *cia5* and *cia5-C* under LL and HL conditions ($n$ = 3 biological samples, mean ± s.d.). The statistical analyses (two-way ANOVA Tukey's multiple comparison test) are shown in the graph. Exact p-values can be found at the Source Data file. Raw fluorescence and NPQ curves can be seen in Supplementary Fig. 4.

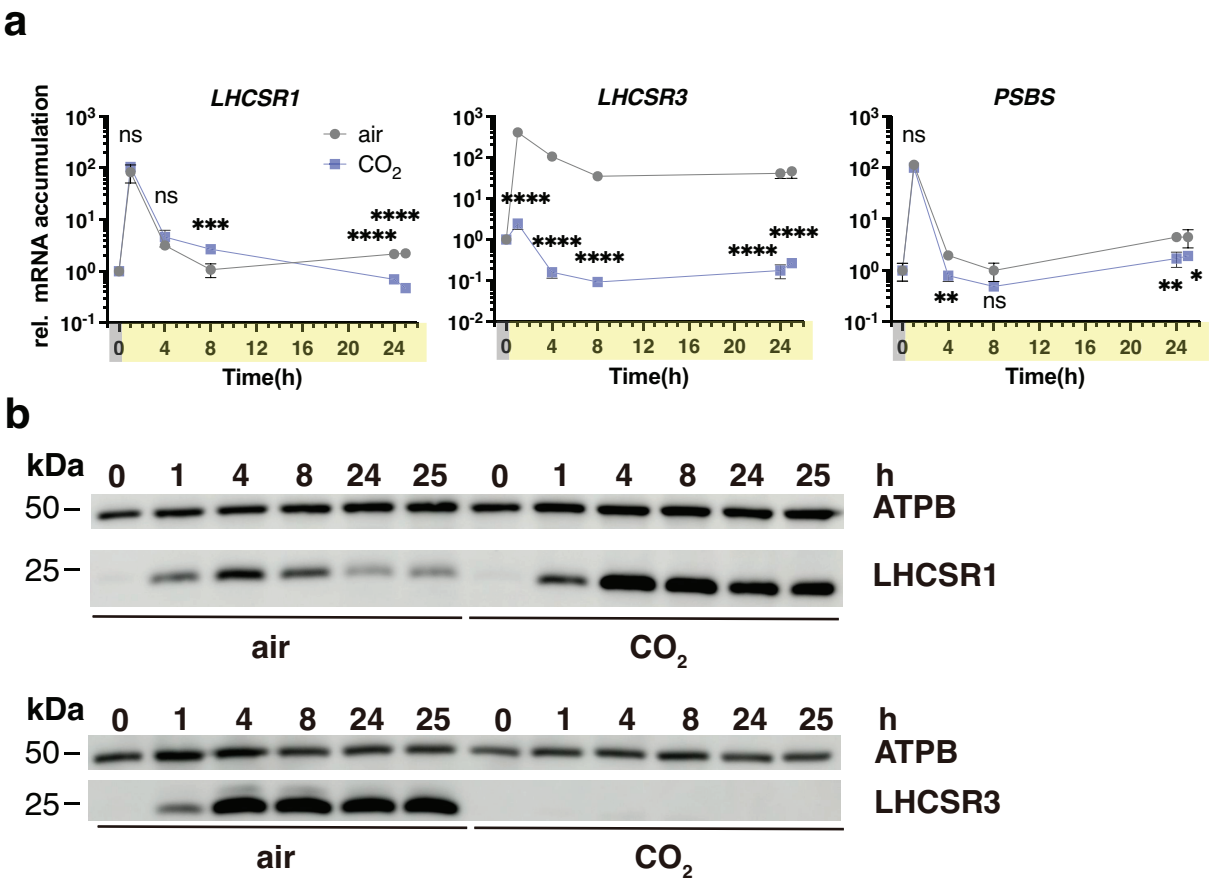


**Figure 4: Kinetic resolution of photoprotective gene and protein expression at different light and $CO_2$ availabilities.** Cells were acclimated overnight at LL (15 µmol photons $m^{-2}$ $s^{-1}$) bubbled with air (labelled "air"). At t=0 the light intensity was raised to 600 µmol photons $m^{-2}$ $s^{-1}$ under air bubbling or bubbling with 5% $CO_2$ and mRNA and protein were followed for 25h. **a** *LHCSR1, LHCSR3* and *PSBS* mRNA accumulation. ($n$ = 3 biological samples, mean ± s.d.). The p-values for the comparisons of $CO_2$ conditions to air for t=1, 4, 8, 24 and 25h are based on two-way ANOVA Šídák's multiple comparisons test of log10 transformed mRNA data as indicated in the graphs (*, $P < 0.005$, **, $P < 0.01$, ***, $P < 0.001$, ****, $P < 0.0001$, ns, not significant). Exact p-values can be found at the Source Data file. **b** Immunoblot analyses of LHCSR1, LHCSR3 and ATPB (loading control). Representative dataset of experiment repeated three times.

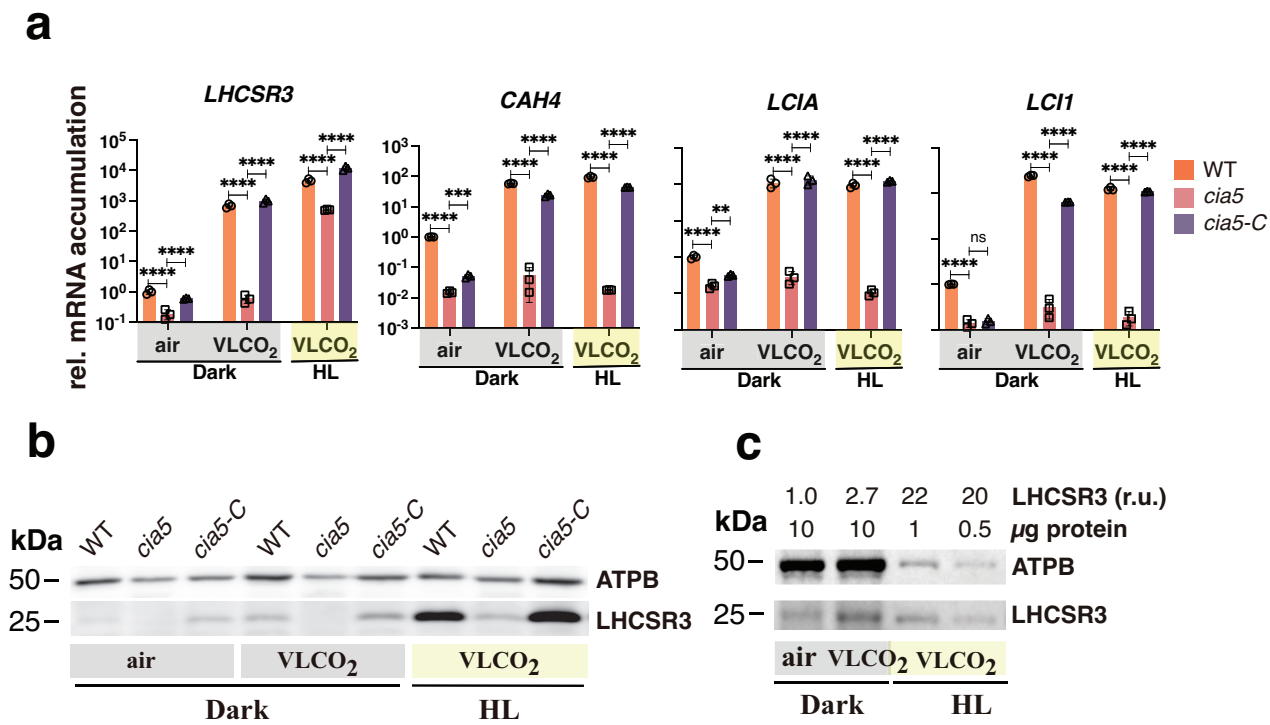


**Figure 5: Low $CO_2$ levels can trigger qE and CCM genes in the absence of light.** WT, *cia5* and *cia5-C* cells were bubbled with air overnight in darkness; next day air bubbling was either maintained or replaced by $CO_2$-limited-air bubbling in the darkness or in the presence of 600 µmol photons $m^{-2}$ $s^{-1}$ light. Sampling was performed after 1 h (RNA) or 4 h (protein). **a** mRNA accumulation of *LHCSR3.1* (qE gene) and *CAH4, LCIA, LCI1* (CCM genes) in WT, *cia5* and *cia5-C*. Data were normalized to WT air dark; ($n$ = 3 biological samples, mean ± s.d.). The p-values for the comparisons of WT with *cia5* and *cia5* with *cia5-C* are based on ANOVA Dunnett's multiple comparisons test of log10 transformed mRNA data as indicated in the graphs (*, P < 0.005, **, P < 0.01, ***, P < 0.001, ****, P < 0.0001, ns, not significant). Exact p-values can be found at the Source Data file. **b** Immunoblot analyses of LHCSR3 and ATPB (loading control) under the indicated conditions. Representative dataset of experiment repeated three times. **c** Immunoblot analyses of LHCSR3 and ATPB (loading control) of WT samples presented in **b**. Above the immunoblot shown are the amount of protein loaded per lane and the quantification of LHCSR3 protein accumulation (calculated as LHCSR3 /ATPB ratio) normalized to the air dark conditions. Representative dataset of experiment repeated three times.

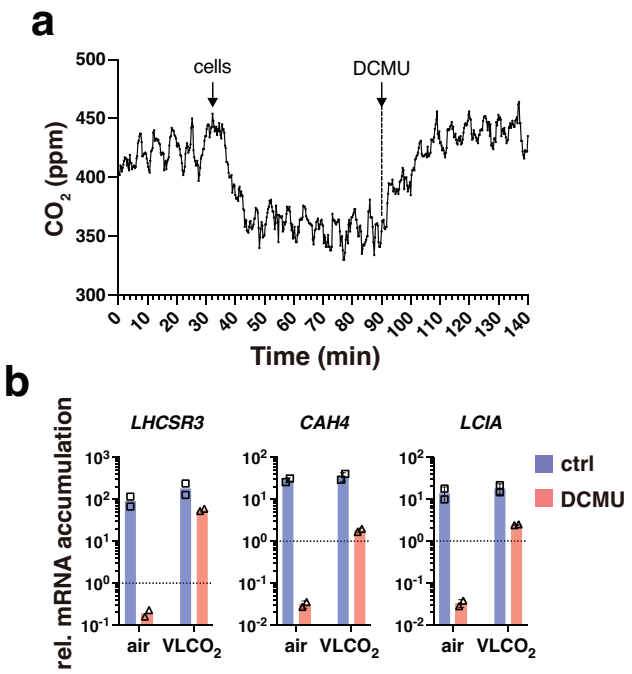


**Figure 6: Photosynthetic electron transfer draws down the intracellular $CO_2$ concentration, relieving inhibition of *LHCSR3* transcription. a** $CO_2$ concentration measured in the air stream coming out of the headspace of a column filled with 50 mL of HSM, sparged with air under HL. The two arrows in the graph indicate the addition of cells or DCMU. **b** WT cells were acclimated to LL HSM overnight shaken in flasks; the next day they were exposed to 300 µmol photons $m^{-2}$ $s^{-1}$ light in the presence or absence of 40 µM DCMU, shaken in flasks without or with sparging with $VLCO_2$. Samples were taken after 1 h. Presented are mRNA accumulation of *LHCSR3*, *CAH4*, *LCIA*. Data were normalized to LL (shown as dotted line in graph); $n = 2$ biological samples.

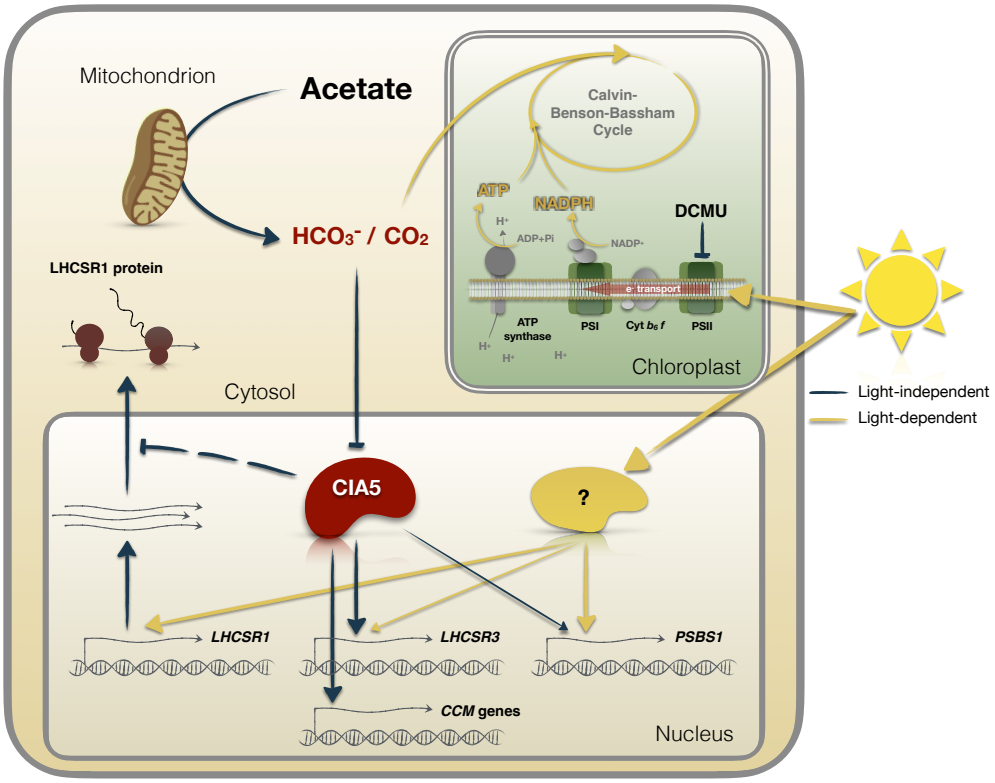


**Figure 7. $CO_2$- and light-dependent signals converge to regulate photoprotection and CCM in Chlamydomonas.** The intracellular levels of $CO_2$, defined by the equilibrium between $CO_2$ fixation in chloroplasts and the generation of $CO_2$ by mitochondrial metabolism (e.g. acetate assimilation) is the key determinant of the regulation of gene expression controlling two major processes of photosynthetic organisms: CCM and photoprotection. Changes in light availability have a direct impact on intracellular $CO_2$ levels; exposure to HL increases $CO_2$ fixation rates leading to depletion of $CO_2$ and to activation of not only photoprotection- but also CCM-related genes. Conversely, depletion of $CO_2$ is sufficient to drive high expression levels of CCM genes and *LHCSR3* even in complete darkness (indicated by the black arrows). High $CO_2$ levels, either exogenously supplied by sparging or metabolically produced via acetate metabolism or by inhibiting photosynthetic electron flow using DCMU, repress *LHCSR3* and CCM genes while at the same time they stabilize LHCSR1 protein levels. The close interconnection of photoprotection and CCM is further corroborated by the fact that CIA5, the regulator of expression of genes associated with the CCM, also exerts control over *LHCSR3* and to a lesser extent over *PSBS* mRNA levels and acts as repressor of LHCSR1 protein accumulation. Independent of CIA5, light strongly impacts expression of all of these photoprotective genes (yellow arrows). This impact can be the consequence of both photoperception (e.g. phototropin) and the production of reactive oxygen species.

# Supplementary Information

**This PDF file includes:**

Supplementary Note 1
Supplementary Figs 1 to 8
Supplementary Tables 1 to 4

**Other Supplementary Materials for this manuscript include the following:**
Supplementary Datasets 1 to 3 (to be downloaded as excel file)

**Supplementary Note 1**

**Application of flux balance analysis to investigate proxies for internal $CO_2$ concentration.** We used flux balance analysis (FBA)[1] to test whether the genome-scale model of *Chlamydomonas i*Cre1355[2] could accurately predict the specific growth rates (generation time) of the *icl* and *dum11* strains under autotrophic LL, autotrophic HL and mixotrophic (acetate) HL conditions. We first constrained the specific growth rates of WT to the measured values under LL and HL[3] and determined the respective minimum photon uptake supporting the specific growth rates (Methods). Assuming that the photon uptake is not altered in the mutants, the determined minimum photon uptake was then used as a bound in the FBA-based prediction of generation times for the *icl* and *dum11* strains. In line with the experimentally observed values, we found that the predicted generation times for the *icl* and *dum11* strains grown autotrophically under LL did not differ from those of LL grown WT cells (**Supplementary Table 1**). In comparison to LL conditions, the predicted generation time of the *icl* and *dum11* strains grown autotrophically under HL decreased by 1.8- and 1.6-fold, respectively, which was also similar to that of WT cells (**Supplementary Table 1**). However, the predicted generation time for the WT grown under mixotrophic HL conditions further declined by 2-fold, to 11 h while the mutants under mixotrophic HL conditions had a generation time similar to that observed under autotrophic HL conditions (19 h, **Supplementary Table 1**). These findings showed that the FBA-based modeling with the condition-specific constraints can reproduce experimental findings regarding strain- and condition-specific generation times.

We next examined whether the $CO_2$-producing reactions show flux differences between the WT and the mutant strains under the specific growth conditions used. To this end, we followed two strategies, one based on the differences in the flux ranges and another based on the differences in the sampled steady-state flux distributions. By using the first strategy, we found a number of reactions whose steady-state flux ranges did not overlap between the WT and modelled mutants under the investigated conditions (**Supplementary Dataset 1**), suggesting clear redistribution of fluxes between WT and mutant. The second strategy allowed us to identify reactions that showed both significant differences in the distributions of the sampled flux values, using the Kolmogorov-Smirnov test, and significant difference in means between WT and the mutants, based on t-tests (**Supplementary Dataset 2**). The Fisher's exact test was in turn used to assess if the set of reactions showing differences are enriched with $CO_2$-producing reactions. Our findings showed that there is a significant difference (p-value = 0.003) in the flux of $CO_2$-producing reactions between WT and mutants for mixotrophic growth under HL conditions; analogous conclusions were made when only focusing on the $CO_2$-producing reactions in the chloroplast (p-value= 6.4e-04; **Supplementary Table 2**). However, this could not be observed under LL and HL photoautotrophic conditions. In addition, we ask if the observed difference in flux of $CO_2$-producing reactions for the mixotrophic HL condition is a result of (in)activation of certain reactions between WT and mutant. To test this hypothesis, we calculated the Jaccard distance between the sets of active $CO_2$-producing reactions. We found that the set of active reactions is the same for all strains indicated by a Jaccard distance of zero. Next, we aim to investigate if the change in flux for $CO_2$-producing reactions is due to an altered relative contribution of reaction fluxes to production of $CO_2$. Therefore, we compute flux splits[4] and find that the relative contribution cannot explain the difference in the phenotype (**Supplementary Table 3**). To further investigate how this observation may propagate to other pathways, i.e., model subsystems, we investigate which pathways show the largest differences between the mutants and the WT for

mixotrophic growth under HL. As a result, we calculate the percentage of reactions that show a significant difference in flux between WT and mutants only under mixotrophic HL condition (**Supplementary Dataset 3**). We found the highest percentage of reactions with significant change for mixotrophic HL condition, but no change under autotrophic LL and HL, for the following pathways: N-Glycan biosynthesis (100%, 26 reactions) and protein synthesis (100%, 1 reaction), followed by tyrosine metabolism (57%, 4 reactions) and valine, leucine and isoleucine degradation (52%, 17 reactions). In addition, pathways like fatty acid biosynthesis (47%, 29 reactions), nitrogen metabolism (45%, 10 reactions), photosynthesis (44%, 4 reactions) as well as starch and sucrose metabolism (40%, 6 reactions) and glycerolipid metabolism (40%, 138 reactions) fall in the highest ranked pathways with respect to percentage of reactions with significant change for mixotrophic HL. These observed changes in fluxes may be explained by transcriptional reprogramming that affect downstream enzyme abundances who support the flux changes. As demonstrated in our experimental validation, $CO_2$ can serve as a signal for these transcriptional reprogramming. In addition, other mechanisms related to allosteric regulation of reaction rates cannot be excluded.

Prompted by these findings, we interrogated whether or not changes in flux are associated with changes in the internal $CO_2$ concentration. Since FBA cannot be used to predict concentrations of metabolites, we used a technique employed in the design of metabolic engineering strategies to modulate the production (and hence concentration) of a metabolite of interest. This technique entails insertion of a synthetic 'demand' reaction for the metabolite of interest, which exports the metabolite out of the network. In our case, we inserted a demand reaction for $CO_2$ from the chloroplast to the environment, and used its maximum flux, at the specific condition associated with strain-specific-growth constraints, as a proxy for intracellular $CO_2$. We then inspected the condition-specific flux through the added demand reaction for different combinations of $CO_2$ and acetate uptake rates (**Supplementary Fig. 2**). We observed the same flux pattern for the $CO_2$ demand reaction with varying rates of $CO_2$ uptake from the environment across all strains under autotrophic LL and HL. We hypothesized that under LL more $CO_2$ can accumulate because of slow carbon fixation in comparison to HL conditions, where $CO_2$ fixation is faster. In support of this hypothesis, we found that all strains showed larger flux through the $CO_2$ demand reaction, as a proxy for the internal $CO_2$ levels, under LL than HL conditions when the $CO_2$ uptake rates were larger than 0.2 mmol/gDW/h (**Supplementary Fig. 2a-c**). Under mixotrophic HL conditions, with the assumption of no change in $CO_2$ uptake from the environment and a decrease of at least 10% in acetate uptake for both mutants in comparison to WT, we found that both the *icl* and *dum11* mutants showed smaller flux through the $CO_2$ demand reaction, i.e. lower internal $CO_2$ concentration than what was observed for WT (**Supplementary Fig. 2d-f**). Furthermore, the same pattern holds with the assumption that $CO_2$ uptake under HL is at least as high as under LL and acetate uptake rates are below 0.3 mmol/gDW/h. In contrast, only few combinations of $CO_2$ and acetate uptake rates for which the mutant strains showed $CO_2$ demand that is similar under autotrophic LL and mixotrophic HL conditions, but larger than the $CO_2$ demand in the WT under auxotrophic LL conditions. Therefore, we concluded that larger $CO_2$ demand flux under autotrophic LL than HL conditions for each strain can be observed with the assumptions that: (i) the $CO_2$ uptake was not affected by the mutation, (ii) $CO_2$ uptake is the same for phototrophic HL and mixotrophic HL, (iii) $CO_2$ uptake under HL is at least as high as under LL and (iv) the acetate uptake rate is low (i.e., below 0.3 mmol/gDW/h) for the mutants (as indicated in **Fig. 2c** and **f**). Moreover, under mixotrophic HL conditions, both mutants exhibited $CO_2$ demand rates that were smaller than those under autotrophic LL conditions. In contrast, the WT showed a marked increase

in the $CO_2$ demand flux under mixotrophic HL conditions in comparison to autotrophic LL and HL, indicating higher internal $CO_2$ concentrations in the presence of acetate. In conclusion, genome-scale metabolic modelling supports the hypothesis that there are changes in the internal $CO_2$ concentration under autotrophic and mixotrophic growth conditions at different light intensities. These changes are congruent with the changes in the accumulation of *LHCSR3* transcripts under the different media conditions and in the WT and mutant cells.

*Condition and strain-specific metabolic models*

Simulations of different strain, $s = \{WT, icl, dum11\}$, and conditions, $c = \{LL, HL, HL + \ acetate\}$, are based on the genome-scale metabolic network reconstruction *i*Cre1355 of *Chlamydomonas reinhardtii* metabolism [2]. The reconstruction provides the underlying structure of the metabolic reactions captured in the stoichiometric matrix, $\boldsymbol{N}$, where rows correspond to metabolites and columns denote reactions. Each entry in the stoichiometric matrix indicates the molarity with which a metabolite is consumed (negative value) or produced (positive value) by the respective reaction. In addition, condition-specific lower and upper bounds on reaction flux, $v_{min}^{WT,c} \leq v \leq v_{max}^{WT,c}$, for autotrophic (LL, HL) and mixotrophic (HL + acetate) growth are provided with the model. To obtain models for the mutants *icl* and *dum11* we used the gene-protein-reaction rules, provided along the network reconstruction, to identify reactions related to knocked-out genes Cre06.g282800 and CreMt.g000300, respectively. Gene Cre06.g282800 relates to reaction isocitrate lyase and therefore, flux through this reaction is blocked in the simulations of *icl*. For the mutant *dum11* the knocked-out gene CreMt.g000300 was not part of the model. However, it is known that this mutant shows no activity of respiratory complex III, therefore the corresponding model reaction was blocked in the simulation of *dum11*.

The strain and condition-specific simulations, together with constraint-based modeling approaches were used to investigate steady state flux distributions, $v$. First, we used the WT model under autotrophic conditions to obtain estimates for photon uptake rates under LL and HL conditions, later used as constraints in the mutant models and for the WT model under HL + acetate condition. Therefore, we take generation time ($g$) of *Chlamydomonas* WT under LL and HL measured by Bonente et al. [3] and converted them into growth rates (μ) assuming that $g = \frac{log(2)}{\mu}$. The respective growth rate was used to constrain the WT model under LL and HL conditions. To estimate photon uptake in units mmol $gDW^{-1}$ $h^{-1}$ under low and high light conditions, we found the minimum photon uptake rate that supports the condition-specific WT growth rate ($bio_c^{WT}$) under LL and HL, respectively (Eq. 1). The resulting photon uptake rates were used as constraints for the simulation of mutants as well as under HL mixotrophic growth for the WT (were no measured growth rates were available). The following is the linear program that we solve:

$$
\begin{aligned}
& z_{photon_{uptake}}^{c} = \min v_{photon_{uptake}} \\
& s.t. \\
& Nv = 0 \qquad\qquad (1) \\
& v_{bio} = bio_c^{WT} \\
& v_{min}^{WT,c} \leq v \leq v_{max}^{WT,c} .
\end{aligned}
$$

Next, we used the observation that mutants cannot grow on acetate in darkness to find acetate uptake rates that allow simulation of no growth in darkness for both mutants. Acetate uptake for both mutants were reduced by 90% in comparison to the WT rate (0.2 mmol $gDW^{-1}$ $h^{-1}$ in mutants and 2 mmol $gDW^{-1}$ $h^{-1}$ in WT), since this rate is the minimum uptake rate for which no growth was simulated in darkness.

*Flux balance analysis*

To simulate maximal growth rates for WT under HL + acetate as well as *icl* and *dum11* under LL, HL and HL + acetate respectively, we applied flux balance analysis (FBA; [5,6]) We found maximal growth rates (Eq. 2) by using the model biomass reaction for mixotrophic and photoautotrophic growth and the respective light constraints. Moreover, acetate uptake for mutant models under HL + acetate was set to 0.2 mmol $gDW^{-1}$ $h^{-1}$, the minimum acetate uptake rate for which no growth was simulated in darkness. To this end, we used the following program:

$$\begin{aligned} & z_{bio}^{s,c} = \max v_{bio} \\ & s.t. \\ & Nv = 0 \\ & v_{photon_{uptake}} = z_{photon_{uptake}}^{c} \\ & v_{min}^{s,c} \leq v \leq v_{max}^{s,c}. \end{aligned} \qquad (2)$$

*Flux ranges*

The solution of the linear programming problem in Eq. (2), above, is the maximum growth, i.e. flux value of the strain and condition-specific biomass reaction, $z_{bio}^{s,c}$. Flux variability analysis (FVA) allows determining the minimum and the maximum value of flux that a given reaction can carry while ensuring maximum flux through the biomass reaction[7]. These values can be obtained by solving the following linear program for a given reaction $i$. The flux through the condition-specific biomass reaction was set to 99% of the optimum to avoid numerical instabilities. To conduct FVA, we solved the following linear programs:

$$\begin{aligned} & z_{i,\max(\min)}^{s,c} = \max(\min)\ v_i \\ & \text{s.t.} \\ & Nv = 0 \\ & v_{photon_{uptake}} = z_{photon_{uptake}}^{c} \\ & v_{min}^{s,c} \leq v \leq v_{max}^{s,c} \\ & v_{bio} = z_{bio}^{s,c} * 0.99 \end{aligned} \qquad (3)$$

Moreover, we sample 5000 feasible steady-state flux distributions from the flux cone of the strain and condition-specific models by applying the function *gpSampler* from the COBRA toolbox[8]. Here, too, biomass was set to 99% of its optimum.

*Non-overlapping flux ranges*

Flux ranges between wild type and mutants are considered to not overlap for condition $c$ if (1) $z_{i,\max}^{WT,c} < z_{i,\min}^{\{icl,dum11\},c}$ or $z_{i,\max}^{\{icl,dum11\},c} < z_{i,\min}^{WT,c}$ , i.e. the minimum flux obtained from FVA (see Eq. 3) in a mutant is larger than the maximum flux obtained for the wild type or the minimum flux in the wild type is larger than the maximum flux for the mutant; i.e. there is no intersection between the flux ranges; (2) minimum flux for WT and mutants is greater than 0.01 mmol $gDW^{-1}$ $h^{-1}$, to avoid considering reactions with low absolute flux; and (3) in line with differential expression analysis, where one considers genes differentially expressed above a preselected fold-change (e.g. of at least 2, in nominal values), for the flux ranges that do not overlap, we use a threshold on the relative difference between the lower bounds of at least 5% (we used 5% to be less restrictive) to filter for cases were flux ranges are close to each other; this condition is meant to remove any numerical artifacts.

*Maximize $CO_2$ demand*

We introduce a demand reaction for $CO_2$ in the chloroplast and maximize its flux given constraints described in the linear program in Eq. (4), which include the fixation of condition-specific growth as well as uptake rates of $CO_2$ and acetate. The obtained flux through $CO_2$ demand will serve as a proxy for internal $CO_2$ concentration in the chloroplast:

$$
\begin{aligned}
& z^c = \max\ v_{CO_2\ demand} \\
& \text{s.t.} \\
& Nv = 0 \\
& v_{photon_{uptake}} = z^c_{photon_{uptake}} \\
& v_{CO_2\ uptake} = CO_2\ uptake^c \qquad (4) \\
& v_{acetate\ uptake} = acetate\ uptake^c \\
& v^{s,c}_{min} \le v \le v^{s,c}_{max} \\
& v_{bio} = z^{s,c}_{bio} * 0.99
\end{aligned}
$$

**Supplementary References**


1. Varma, A. & Palsson, B. O. Metabolic capabilities of Escherichia coli: I. synthesis of biosynthetic precursors and cofactors. *J. Theor. Biol.* **165,** 477–502 (1993).
2. Imam, S. *et al.* A refined genome-scale reconstruction of Chlamydomonasmetabolism provides a platform for systems-level analyses. *Plant J.* **84,** 1239–1256 (2015).
3. Bonente, G., Pippa, S., Castellano, S., Bassi, R. & Ballottari, M. Acclimation of Chlamydomonas reinhardtii to different growth irradiances. *J. Biol. Chem.* (2011). doi:10.1074/jbc.M111.304279
4. Aurich, M. K., Fleming, R. M. T. & Thiele, I. MetaboTools: A Comprehensive Toolbox for Analysis of Genome-Scale Metabolic Models. *Front Physiol* **7,** 327 (2016).
5. Orth, J. D., Thiele, I. & Palsson, B. Ø. What is flux balance analysis? *Nat. Biotechnol.* **28,** 245–248 (2010).
6. Bordbar, A., Monk, J. M., King, Z. A. & Palsson, B. Ø. Constraint-based models predict metabolic and associated cellular functions. *Nat. Rev. Genet.* **15,** 107–120 (2014).
7. Gudmundsson, S. & Thiele, I. Computationally efficient flux variability analysis. *BMC Bioinformatics* **11,** 489–3 (2010).
8. Heirendt, L. *et al.* Creation and analysis of biochemical constraint-based models using the COBRA Toolbox v.3.0. *Nature Protocols* **14,** 639–702 (2019).

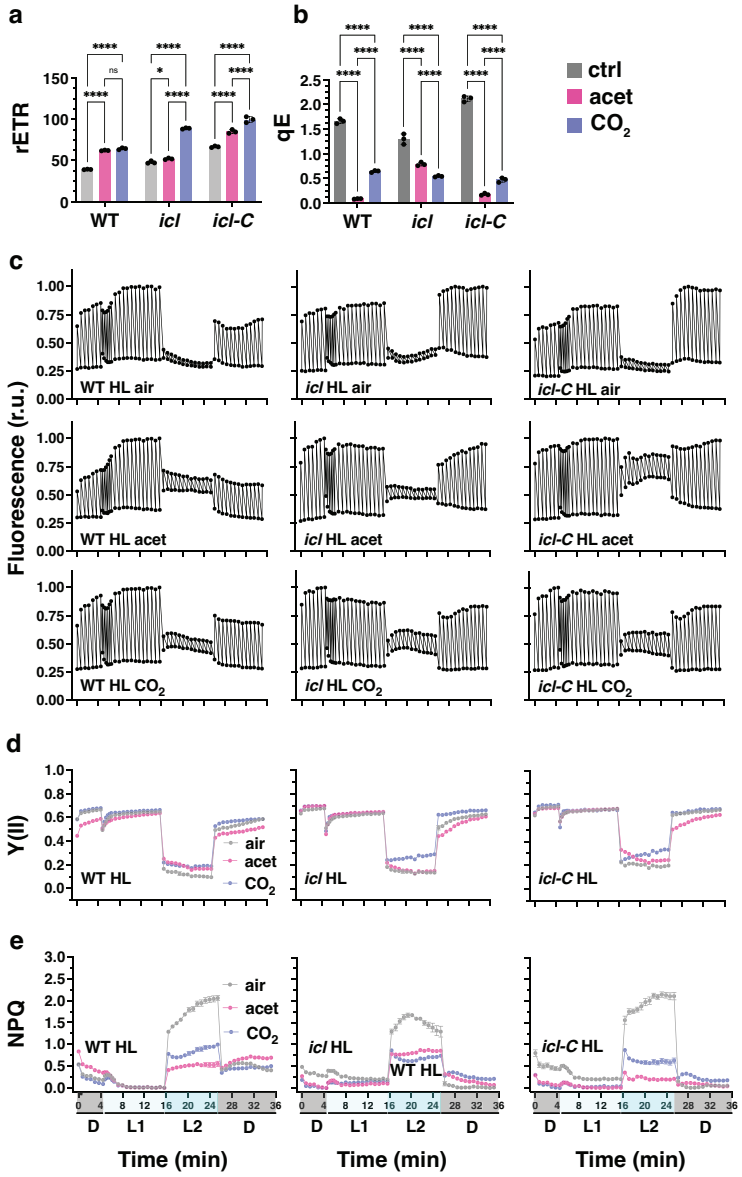


**Supplementary Fig. 1: Effect of carbon availability on the photosynthetic properties of WT, *icl* and *icl-C* cells. a** relative photosynthetic electron transfer rETR measured at 336 µmol photons $m^{-2}$ $s^{-1}$ and **b** qE of WT, *icl* and *icl-C* cells exposed to 600 µmol photons $m^{-2}$ $s^{-1}$ in HSM for 4h; sparged with air (labelled as "air"); sparged with air and supplemented with 10 mM sodium acetate (labelled as "acet); sparged with air enriched with 5% $CO_2$ (labelled as "$CO_2$"), ($n$ = 3 biological samples, mean ± s.d.). The statistical analyses (two-way ANOVA with Tukey's multiple comparisons tests) of **a** and **b** are shown in the graph; * = $P$ value < 0.05, ***=P value <0.001. Exact p-values can be found at the Source Data file. **c** Raw data of *in vivo* chlorophyll fluorescence (normalized to the highest Fm') for WT, *icl* and *icl-C*. Chlorophyll fluorescence was recorded in the dark (labelled as "D"), at 21 (labelled as "L1") and 336 (labelled as "L2") µmol photons $m^{-2}$ $s^{-1}$ as indicated in the graphs. Shown are one representative trace of three biological replicates. **d** Y(II) values calculated as (Fm'-F)/Fm' ($n$ = 3 biological samples, mean ± s.d.). **e** NPQ values calculated as ($F$m − $F$m′)/$F$m ($n$ = 3 biological samples, mean ± s.d.). Please not that in **d** and **e** most of the error bars are smaller than the data points and are therefore not visible.

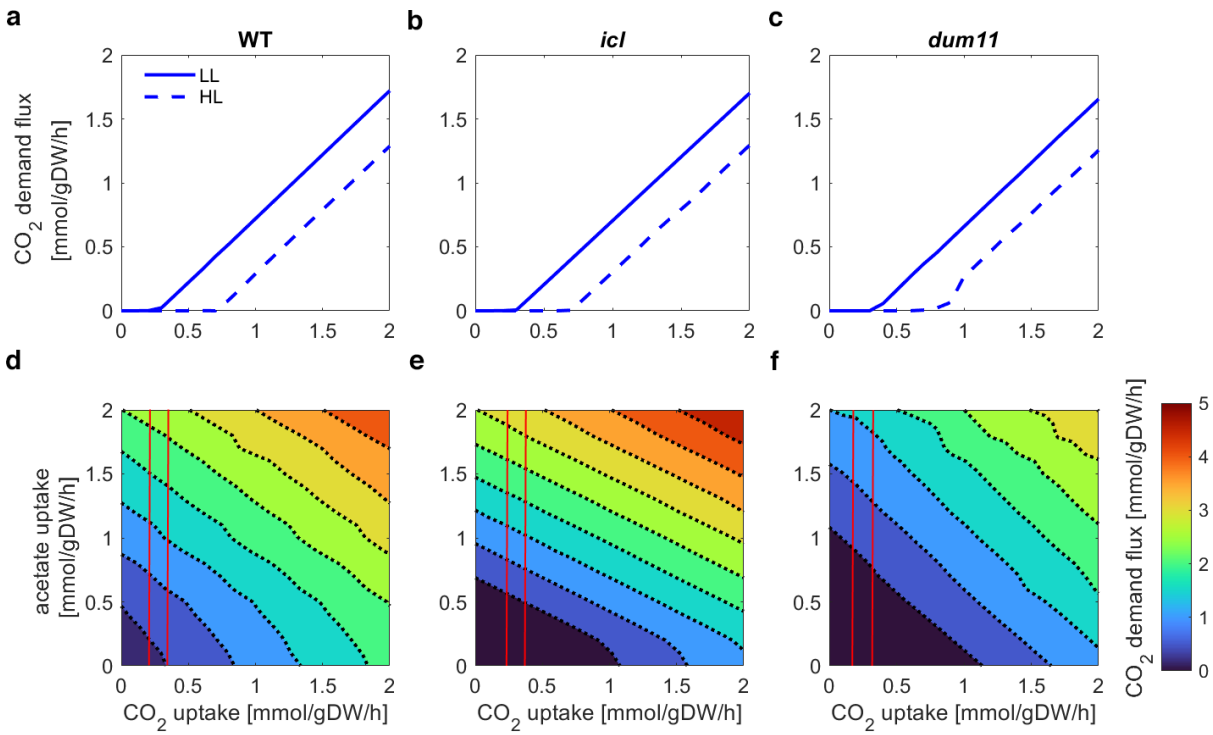


**Supplementary Fig. 2: Large-scale metabolic modeling supports the change in internal $CO_2$ concentration under mixotrophic conditions.** The maximum flux through the $CO_2$ demand reaction is used as a proxy for concentration of free $CO_2$ in the chloroplast. **a-c** Flux through $CO_2$ demand reaction under low light (LL) and high light (HL) for varying $CO_2$ uptake rates for wild type (wt), *icl*, and *dum11*. **d-f** Contour plots of flux through $CO_2$ demand reaction under HL and acetate for varying $CO_2$ and acetate uptake rates for the three respective strains. The area between the two red lines indicates combinations of $CO_2$ and acetate uptake rates that show (i) in the case of mutants: $CO_2$ demand level under HL acetate conditions similar to those under LL conditions and (ii) in the case of the WT: $CO_2$ demand level under HL acetate conditions above what is observed under LL conditions.

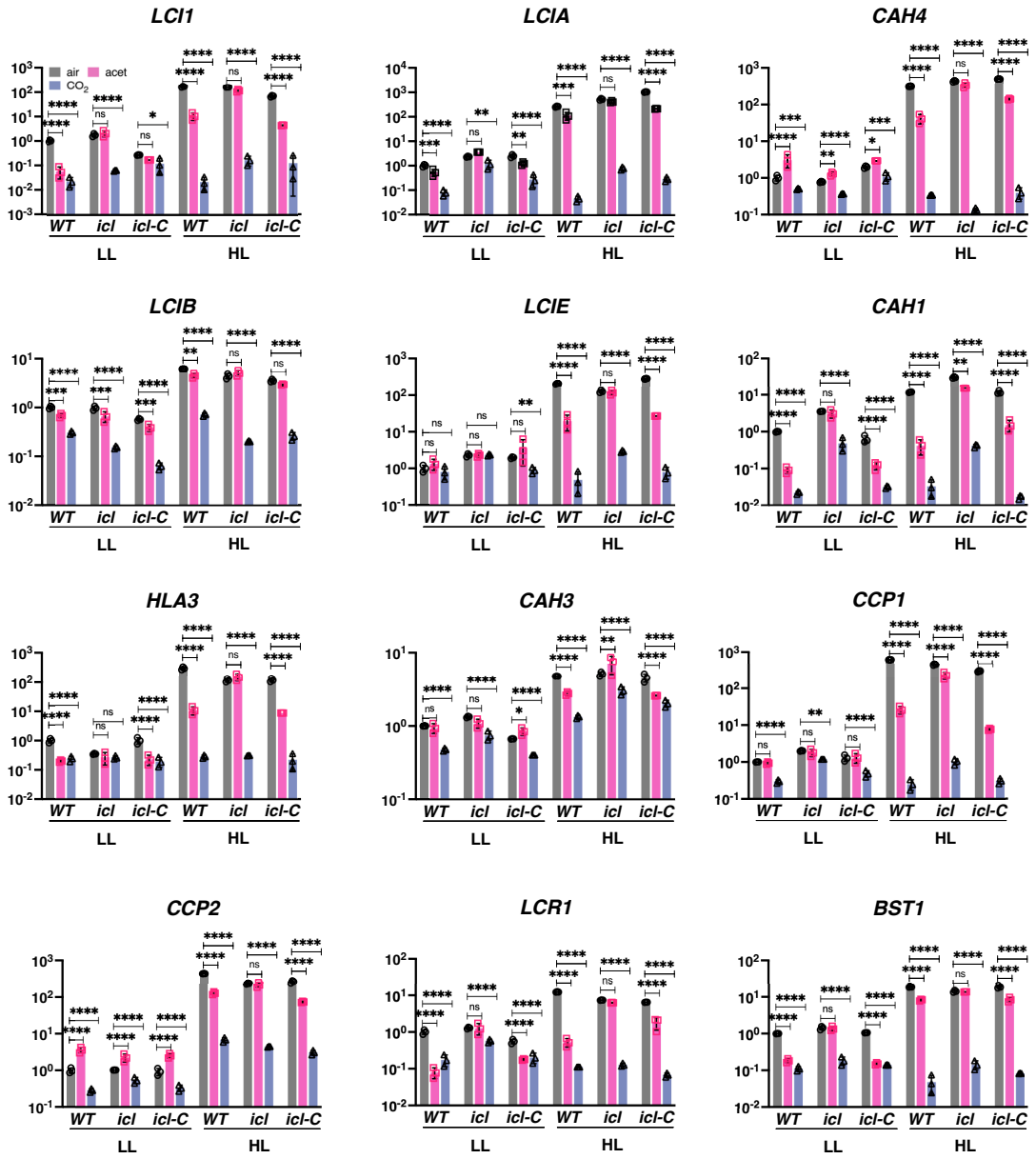


**Supplementary Fig. 3: HL and low-$CO_2$ responses cross-talk.** WT, *icl* and *icl-C* strains were acclimated for 16 h in LL (15 µmol photons $m^{-2}$ $s^{-1}$) in HSM; bubbled with air (labelled "ctrl"); bubbled with air and supplemented with 10 mM sodium acetate (labelled "acet); bubbled with air enriched with 5% $CO_2$ (labelled "$CO_2$"). After sampling for the LL conditions, light intensity was increased to 600 µmol photons $m^{-2}$ $s^{-1}$ (HL); samples were taken after 1h. Accumulation of mRNA of selected CCM genes at the indicated conditions normalized to WT LL ctrl. Please note that these data derive from analyses of the RNA samples of the experiment described in **Fig. 1** ($n$ = 3 biological samples, mean ± s.d.). The p-values for the comparisons of acetate and $CO_2$ conditions to air are based on ANOVA Dunnett's multiple comparisons test of log10 transformed mRNA data as indicated in the graphs (*, $P < 0.005$, **, $P < 0.01$, ***, $P < 0.001$, ****, $P < 0.0001$, ns, not significant). Exact p-values can be found at the Source Data file.

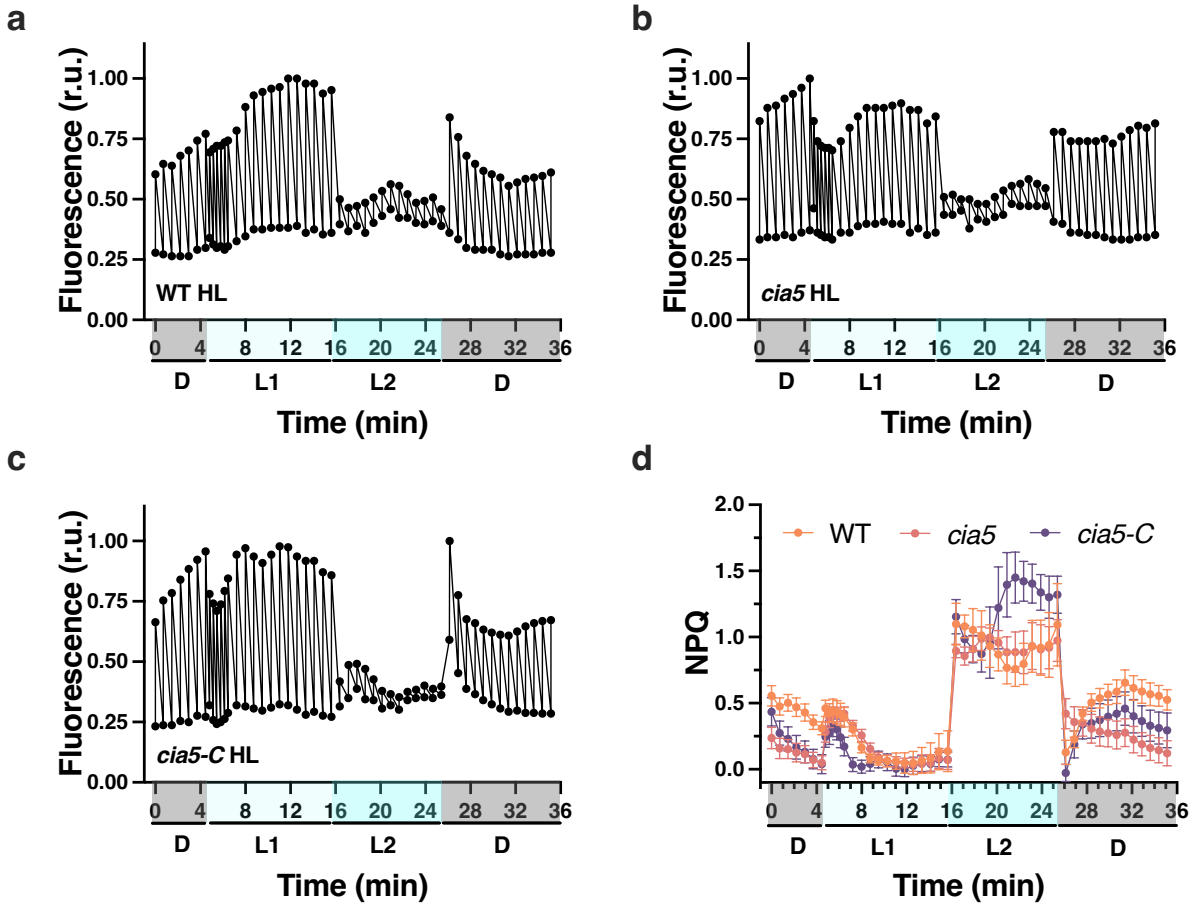


**Suppementary Fig. 4: Detailed view of photosynthetic measurements of Fig. 3c.**
WT, *cia5* and *cia5-C* strains were acclimated for 16 h in LL (15 µmol photons $m^{-2}$ $s^{-1}$) in HSM bubbled with air (labelled as "LL"); after sampling for the LL conditions, light intensity was increased to 600 µmol photons $m^{-2}$ $s^{-1}$ (HL); samples were taken after 4 h for photosynthesis measurements). **a-c** *In vivo* chlorophyll fluorescence (normalized to the highest Fm') of HL-acclimated WT, *cia5* and *cia5-C* cells (for a complete description of the experimental setup please refer to the legend of **Fig. 4**.) Just prior to the onset of the measurements, cells were acclimated to darkness for 15 min. Chlorophyll fluorescence was recorded in the dark (labelled as "D"), at 21 (labelled as "L1") and 336 (labelled as "L2") µmol photons $m^{-2}$ $s^{-1}$ as indicated in the graphs. **d** NPQ values calculated as $(Fm - Fm')/Fm'$ ($n$ = 3 biological samples, mean ± s.d.).

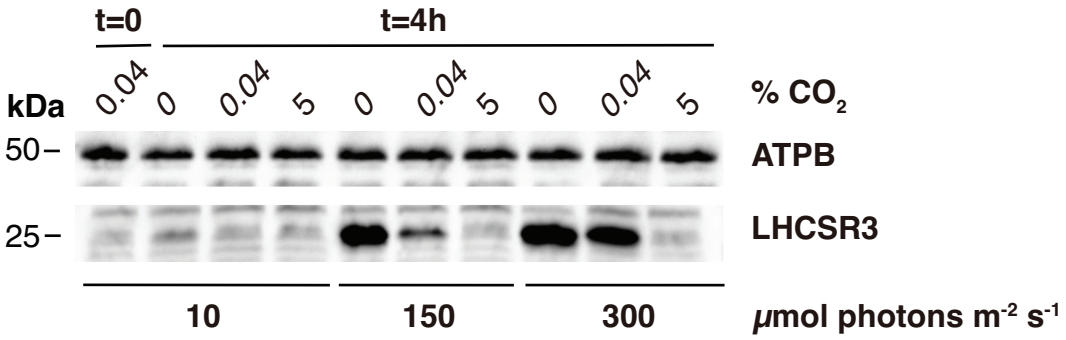


**Supplementary Fig. 5: Light and $CO_2$ availability define expression levels of LHCSR3**. WT cells, acclimated in LL (10 µmol photons $m^{-2}$ $s^{-1}$) sparged with air were shifted to 10, 150, and 300 µmol photons $m^{-2}$ $s^{-1}$ of light and were sparged with 0 (100% $O_2$), 0.04 (air), and 5% $CO_2$ (95% $O_2$) for 4 hours. Shown are the immunoblot analyses of LHCSR3 and ATPB (loading control) under the indicated conditions. Representative dataset of experiment repeated three times.

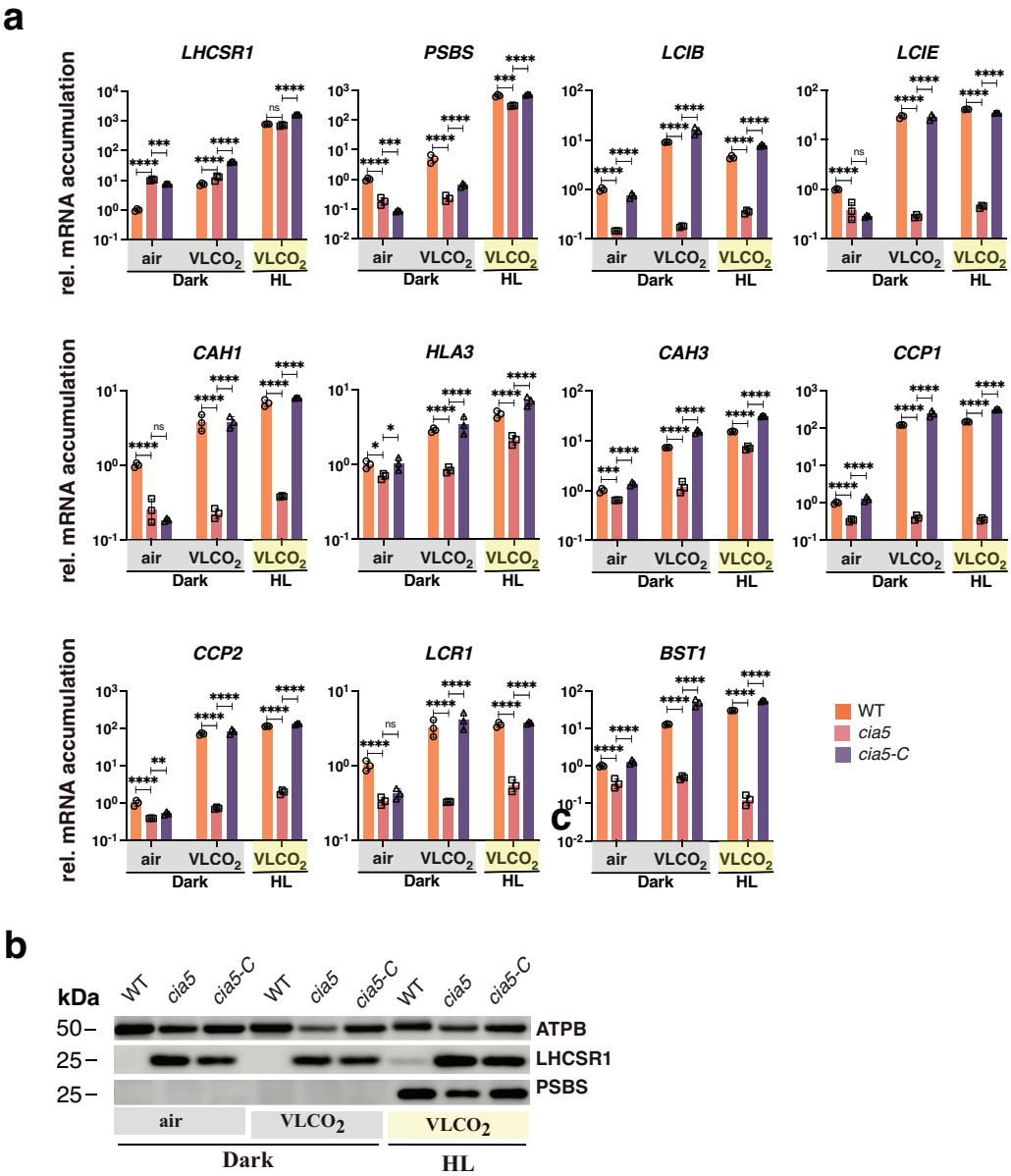


**Supplementary Fig. 6: Low $CO_2$ levels can trigger CCM genes in the absence of light.** WT, *cia5* and *cia5-C* cells were bubbled with air overnight in darkness; next day air bubbling was either maintained or replaced by $CO_2$-limited-air bubbling in the darkness or in the presence of 600 µmol photons $m^{-2}$ $s^{-1}$ light. Sampling was performed after 1 h (RNA) or 4 h (protein). **a** mRNA accumulation of *LHCSR1* and *PSBS1* (qE genes) and *LCIB, LCIE, CAH1, HLA3, CAH3, CCP1, CCP2, LCR1, BST1* (CCM genes) in WT, *cia5* and *cia5-C*. Data were normalized to WT air dark; ($n$ = 3 biological samples, mean ± s.d.). The p-values for the comparisons of WT with *cia5* and *cia5* with *cia5-C* are based on ANOVA Dunnett's multiple comparisons test of log10 transformed mRNA data as indicated in the graphs (*, P < 0.005, **, P < 0.01, ***, P < 0.001, ****, P < 0.0001, ns, not significant). Exact p-values can be found at the Source Data file. **b** Immunoblot analyses of LHCSR1, PSBS and ATPB (loading control) under the indicated conditions.

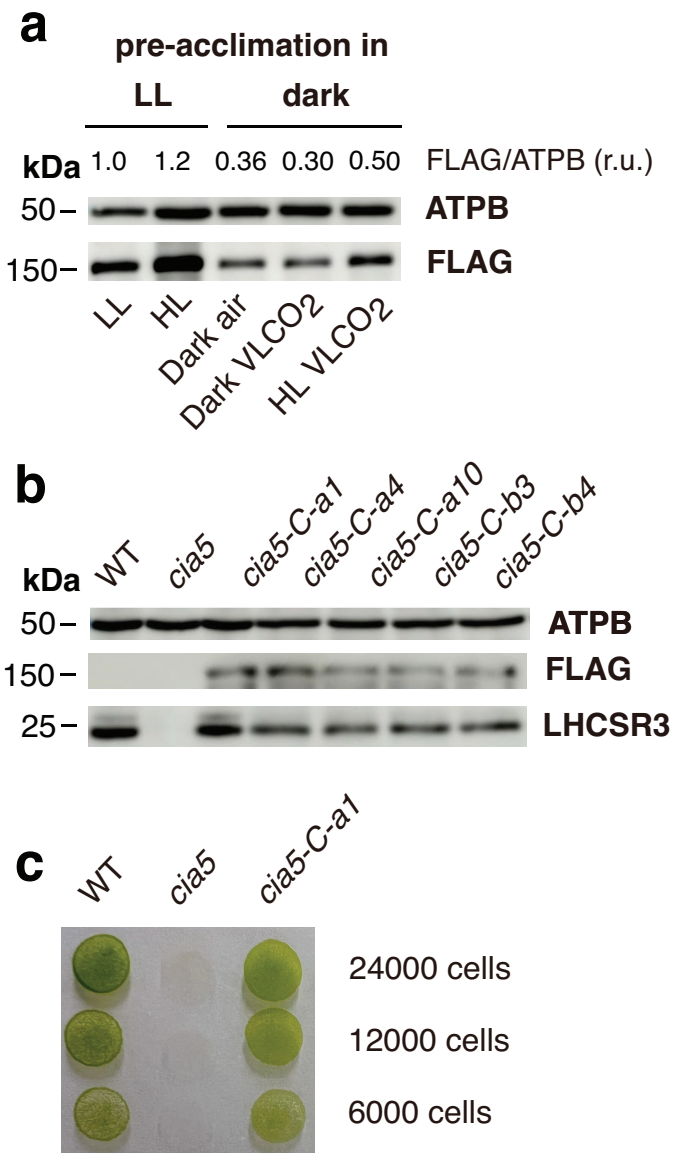


**Supplementary Fig. 7: Complementation of *cia5* mutant. a** Immunoblot analyses of CIA5-FLAG and ATPB (loading control) from whole cell extracts of *cia5-C*. The first two lanes, were loaded with *cia5-C* samples from the experiment presented in **Fig. 3b** (pre-acclimated in LL); the last three lanes contain *cia5-C* samples from the experiment presented in **Fig. 5b** (pre-acclimated in the dark). Above the immunoblot shown is the quantification of CIA5-FLAG protein accumulation (calculated as FLAG /ATPB ratio). Representative dataset of experiment repeated three times. **b** Immunoblot analyses of LHCSR3, CIA5-FLAG and ATPB (loading control) from whole cell extracts of WT, *cia5* and four *cia5-C* complemented lines after exposure at 300 µmol photons $m^{-2}$ $s^{-1}$ for 4 hours. Among the transformants analyzed the *cia5-C-a1* (*cia5-C* throughout the text) was retained for further analyses in the present study. Representative dataset of experiment repeated three times. **c** A total of 24, 12 and 6 x $10^3$ cells of WT, *cia5* and *cia5-C-a1* were spotted on high-salt media agar plates and grown under 100 µE $m^{-2}$ $s^{-1}$ for four days.

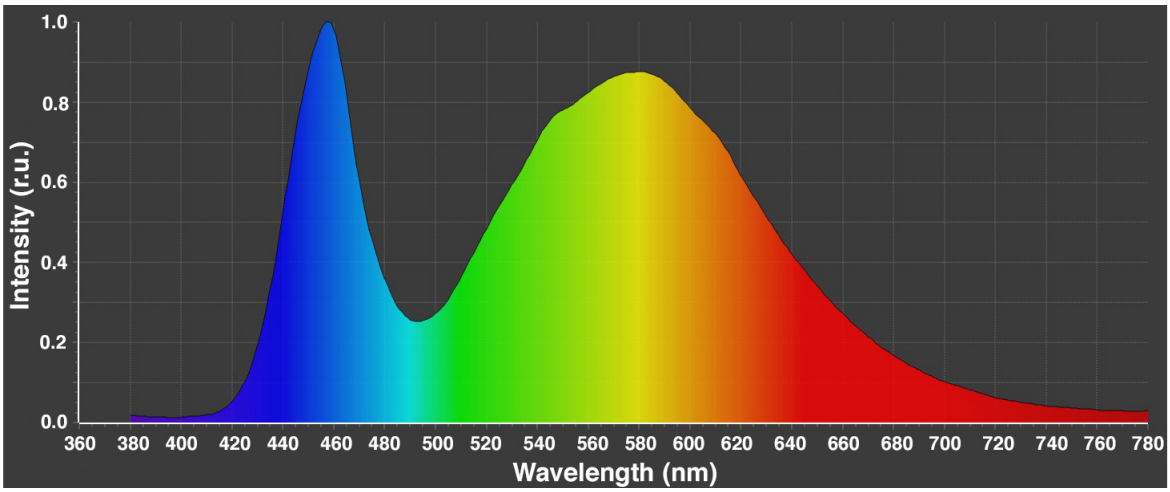


**Supplementary Figure 8:** Light Spectrum of the LED light system (Neptune L.E.D., France) used in the present study.

**Supplementary Table 1. Predicted and observed generation time (h) for wild type and mutant strains under different growth conditions.** Wild type and mutant strains were grown photoautotrophically under low light (LL) and high light (HL) conditions and cells grown mixotrophically on HSM medium were supplemented with acetate under high light (HL + acetate) conditions. Values followed by an asterisk represent constraints based on measurements, the rest of the values were simulated.

| | **LL** | **HL** | **HL + acetate** |
|---|---|---|---|
| **WT** | 36* | 20* | 11 |
| ***icl*** | 36 | 20 | 19 |
| ***dum11*** | 36 | 22 | 19 |

**Supplementary Table 2. Overview number of reactions producing $CO_2$ with significant changes in flux between mutants (*icl* and *dum11*) and WT.** (A) Across all model reactions; (B-D) compartment-specific reactions producing $CO_2$ - (B) cytosol, (C) chloroplast, (D) mitochondria. A significant enrichment in reactions with flux differences between mutants and WT for reactions that produce $CO_2$ under HL + acetate conditions (based on two-sided Fisher exact test) only was observed considering reactions in the chloroplast and considering all model.

**A – all model reactions**

| | $CO_2$ producing | not $CO_2$ producing | p-value |
|---|---|---|---|
| **LL condition** | | | |
| change in flux | 24 | 499 | 0.13 |
| no change in flux | 64 | 1807 | |
| **HL condition** | | | |
| change in flux | 19 | 504 | 0.57 |
| no change in flux | 69 | 1802 | |
| **HL + acetate condition** | | | |
| change in flux | 59 | 1186 | **0.003** |
| no change in flux | 29 | 1120 | |

**B - cytosol**

| | $CO_2$ producing | not $CO_2$ producing | p-value |
|---|---|---|---|
| **LL condition** | | | |
| change in flux | 7 | 313 | 0.48 |
| no change in flux | 24 | 1192 | |
| **HL condition** | | | |
| change in flux | 7 | 318 | 0.49 |
| no change in flux | 24 | 1187 | |
| **HL + acetate condition** | | | |
| change in flux | 18 | 840 | 0.48 |
| no change in flux | 13 | 665 | |

**C - chloroplast**

| | $CO_2$ producing | not $CO_2$ producing | p-value |
|---|---|---|---|
| **LL condition** | | | |
| change in flux | 9 | 71 | 0.37 |
| no change in flux | 21 | 206 | |
| **HL condition** | | | |
| change in flux | 8 | 68 | 0.48 |
| no change in flux | 22 | 209 | |
| **HL + acetate condition** | | | |
| change in flux | 24 | 133 | **6.4e-04** |
| no change in flux | 6 | 144 | |

**D - mitochondria**

| | $CO_2$ producing | not $CO_2$ producing | p-value |
|---|---|---|---|
| **LL condition** | | | |
| change in flux | 8 | 80 | 0.45 |
| no change in flux | 17 | 198 | |
| **HL condition** | | | |

| | | | |
|---|---|---|---|
| change in flux | 4 | 70 | 0.9 |
| no change in flux | 21 | 208 | |
| **HL + acetate condition** | | | |
| change in flux | 17 | 138 | 0.06 |
| no change in flux | 8 | 140 | |

**Supplementary Table 3. Relative contribution of reaction flux to production of $CO_2$.** The set of reactions with non-zero contribution is the same for all strains and conditions.

| | LL | | | HL | | | HL+ac | | |
|---|---|---|---|---|---|---|---|---|---|
| Reaction ID | WT | icl | *dum11* | WT | *icl* | *dum11* | WT | *icl* | *dum11* |
| 'HCO3Em' | 0.42 | 0.25 | 0.34 | 0.25 | 0.25 | 0.27 | 0.34 | 0.34 | 0.35 |
| 'ICDH_nad' | 0.38 | 0.49 | 0.29 | 0.49 | 0.50 | 0.45 | 0.28 | 0.29 | 0.28 |
| 'GLYDHD' | 0.19 | 0.25 | 0.35 | 0.25 | 0.24 | 0.27 | 0.35 | 0.35 | 0.35 |
| 'PPCKm' | 0.00 | 0.01 | 0.01 | 0.01 | 0.01 | 0.00 | 0.01 | 0.01 | 0.01 |
| 'HCO3Ehi' | 0.00 | 0.01 | 0.01 | 0.01 | 0.01 | 0.01 | 0.01 | 0.01 | 0.01 |

## Supplementary Table 4. RT-qPCR primers for the genes analyzed in this study

| Gene ID | Gene Name | Sense Primer | Anti-sense Primer |
|---|---|---|---|
| **Cre01.g016600** | PSBS1 | TAAACCGTGTATTGGAACTCCG | CTCTGCACGCGGCGTGTT |
| **Cre08.g367500** | LHCSR3.1 | CACAACACCTTGATGCGAGATG | CCGTGTCTTGTCAGTCCCTG |
| **Cre08.g365900** | LHCSR1 | GAGTCTGAGATCACCCACGG | CCGATCTGCTGGAAGTGGTA |
| **Cre06.g278222** | GBLP | TGGCTTTCTCGGTGGACAAC | CTCGCCAATGGTGTACTTGC |
| **Cre06.g309000** | LCIA | AGATTTGATAACGGCAGGACC | CCTATCCCATGTCATTCCCAC |
| **Cre10.g452800** | LCIB | TGCATAAGAGCGGATGTAGC | CGGTAGTCAGCATCAGTCATC |
| **Cre04.g223250** | LCIE | TGCCGCCATAGATGTTGTGT | CCGCTCTTCTCTTTCGCTCA |
| **Cre09.g399552** | LCR1 | GCACCAGCATACACCAAAATC | CAGAAAACAGAACGACCAAAGC |
| **Cre03.g162800** | LCI1 | TTGCGGTTTTTGTACGAGCG | GTGCAAAGCCACGTCATCTC |
| **Cre02.g097800** | HLA3 | CAGTGGCATGTTCCCTTTTG | GGTGCTCATGGTTCTTGTTTG |
| **Cre03.g162800** | CAH1 | GCTTTGCTTCACGGTTTGGT | CCGGTACTGTGTGTATGCGT |
| **Cre09.g415700** | CAH3 | AACCTGGAAGGGTGTGTGTG | CACTTCTCGAAGCTGCCGTA |
| **Cre05.g248400** | CAH4 | CGAAAAGCTGCATGAACTCACC | GCCCGTAGGCTACAGTTTTC |
| **Cre04.g223300** | CCP1 | TGGCATGACAACATGGCTCA | AGTGCATCCACTGGCTTGTT |
| **Cre04.g222750** | CCP2 | AACGTGGAGCACATCTACGG | ATAAGCCGTCAAGCCTTGCT |
| **Cre16.g662600** | BST1 | GCTGTGTGGCATTGAGGAGA | GGATGAGGCTGATGAGTCCG |
| **Cre06.g284100** | RHP1 | GCAGTCGCAGGCAGTAACTA | CGCTTCAGCGCTCATAGAGA |
| **gib-cia5** | | gctactcacaacaagcccagttATGGAAGCCTTAGACGCGC | gagccacccagatctccgttATCGCAGGACTGCAGCAG |

**Supplementary Dataset 1** (available as downloadable Microsoft Excel file). Reactions whose minimum flux in the mutant was above the maximum flux of the WT (up-regulation) or the maximum flux in the mutant was below the minimum observed in the WT (down-regulation). Marked cells for down regulation under HL + acetate represent reactions also down regulated under LL in *dum11*.

**Supplementary Dataset 2** (available as downloadable Microsoft Excel file). Flux ranges obtained from flux variability analysis as well as mean and median flux from sampling of 5000 flux distributions. Reactions marked in green show significant difference under HL+acetate but not under LL and HL conditions.

**Supplementary Dataset 3** (available as downloadable Microsoft Excel file). Percentage of reactions per model pathway that show significant change in sampled flux values in both mutants, *icl* and *dum11* for the respective condition.